VIBRATING CPD CHEMICAL DEGRADATION OIL SENSOR

A Thesis
Presented to
The Academic Faculty

by

Siarhei Tsiareshka

In Partial Fulfillment
of the Requirements for the Degree
Master of Science in the
School of Mechanical Engineering

Georgia Institute of Technology
August 2006

VIBRATING CPD CHEMICAL DEGRADATION OIL SENSOR

Approved by:

Dr. Steven Danyluk, Advisor
School of Mechanical Engineering
Georgia Institute of Technology

Dr. Peter Hesketh
School of Mechanical Engineering
Georgia Institute of Technology

Dr. Thomas Kurfess
School of Mechanical Engineering
Georgia Institute of Technology

Date Approved: May 15, 2006

This thesis is dedicated to everyone who has helped me and supported me to this point in my life: my parents who have been taking care of me, my brother who was and is an excellent example to follow, and all my friends and co-workers. Thank you all.

ACKNOWLEDGEMENTS

I would like to thank everyone who has helped me in my research and in accomplishing this thesis work, first and foremost, my thesis and research advisor Dr. Steven Danyluk for his trust, support, and wise guidance throughout my time working with him.

Dr. Anatoly Zharin, for his support and his knowledge share in the areas of analog circuit design, and tribological topics,

Dr. Jiri Janata and Dr. Mira Josowicz, for helping me with the sample analyses using FTIR and UV-VIs spectrometers,

Vladimir Bortkevich, for advising in the area of circuit design,

Lisa Teasley and Dona Rogers, for making everything run smoothly.

I would like thank everyone in the CPD group, a part of the Electronic Materials Research Laboratory, especially Frank Mess for his advises and insight, Daniel Osorno for helping me with machining. Special thanks to all the folks in the Electronic Materials Research Laboratory for creating a great atmosphere to grow and learn.

I would like to express special thanks to my family for supporting all my attempts and endeavors. Without them, I would never accomplish the things I have already accomplished and the goals I have already achieved. I hope they will always be there for me to support and inspire.

TABLE OF CONTENTS

LIST OF TABLES

LIST OF FIGURES

SUMMARY

This thesis utilized the concept of the vibrating contact potential difference (CPD) measurement to monitor the chemical degradation of oil. The CPD sensor is one variation of the vibrating Kelvin-Zisman method to monitor the differences in surface potential between two metal electrodes. One of the plates that form a capacitor serves as a sampling electrode, on which a film of oil is placed, while the other is electrically isolated by an air gap. The interaction between the oil sample and the electrode surface causes the CPD to change. This change is picked up by the electronics and synchronously measured. The experiment involved placing different samples of an oxidized synthetic lubricant on one electrode and logging the output. The oil samples were prepared by thermal aging in the laboratory environment.

Experiments showed that the sensor was able to distinguish between oil samples with different degrees of oxidation (number of hours during which the oil was oxidized). Moreover the sensor was able to detect depletion of antioxidants and depletion of detergents in the untreated motor oil. The output voltage was related to the adsorption of the oil on the active electrode. A theoretical model based on the Langmuir adsorption isotherm and Helmholtz equation was developed. The model was calibrated by use of the experimental data in order to obtain the model parameters. An important relationship characterizing adsorption of oxidized motor oil on brass was obtained, relating the normal component of dipole moment and area of adsorption. Furthermore, the calculation for the dipole moment of adsorbed oil molecule was done; the value of 0.95D is close to that found in the literature.

CHAPTER 1

INTRODUCTION

This thesis investigates the concept of monitoring oil degradation by the vibrating Kelvin probe technique. The Kelvin method refers to the measurement of the contact potential difference between metals. The contact potential difference or *Contact Electricity of Metals* [1] was first described by Lord Kelvin in 1898. Kelvin investigated the phenomena of contact electricity proposed by Volta [2]. The CPD occurs when two dissimilar metals are brought in proximity. Kelvin used an electrometer to measure the amount of charge flowing from one metal to another and related this charge to the surface potential dissimilarity between the metals. Two metal surfaces in close proximity could be considered to form a parallel plate capacitor. Zisman proposed vibrating one of the plates and measuring the alternating current passing through the capacitor induced by the CPD between the metals [3]. The Kelvin-Zisman method is also known as the vibrating Kelvin method.

The vibrating Kelvin Probe method for measuring the work function of metals has been used since 1932. The determination of the contact potential difference involving this technique has been widely used in various fields of investigation such as: catalysis, adsorption, chemical reactivity at semiconductor surfaces, and so on. Moreover, when using a reference electrode, the vibrating Kelvin probe method leads to an indirect measurement of the electronic work function. The Kelvin-Zisman technique is a very sensitive method for studying electronic characteristics of conductors and their surfaces, especially in the case of continuous measurements. One

of the most significant features is that this technique is sensitive to the work function change on the order of 1 mV. This result is extremely sensitive compared with a shift of about 0.05 V resulting from the coverage of one monolayer of atoms on the surface [6].

A novel application of the above method is proposed in this thesis in a form of a sensor. A flow chart of this work is represented in Figure 1-1. The research involved theoretical model development, design of the experimental setup, and sample preparation. Some of these independent stages consist of sub-stages. Design of the experimental setup itself consists of hardware, software, and electronic circuit designs. As a final point the obtained results for oil were justified by comparison to the values predicted by the theoretical model and that found in the literature.

The vibrating Kelvin probe was created with one static surface acting as a sampling surface and the other electrically isolated. The interaction of the oil with one of the surfaces of a capacitor results in a signal which can be synchronously measured.

Oil molecules adsorb on the surface of one of the plates and change its work function. The magnitude of that change depends on the chemical composition of the oil. Different types of molecules have different adsorption energies, due to the different molecular groups that adsorb on the surface. The fractional coverage of the surface by several types of molecules results in a potential of the adsorbed layer which depends on the concentration of the particular molecular type. Thus, the fraction of the oxidized molecules in the bulk oil is seen as a change in the voltage output of the sensor. Eight oil samples with different levels of oxidation were prepared in the laboratory by the thermal aging at 180^0C.

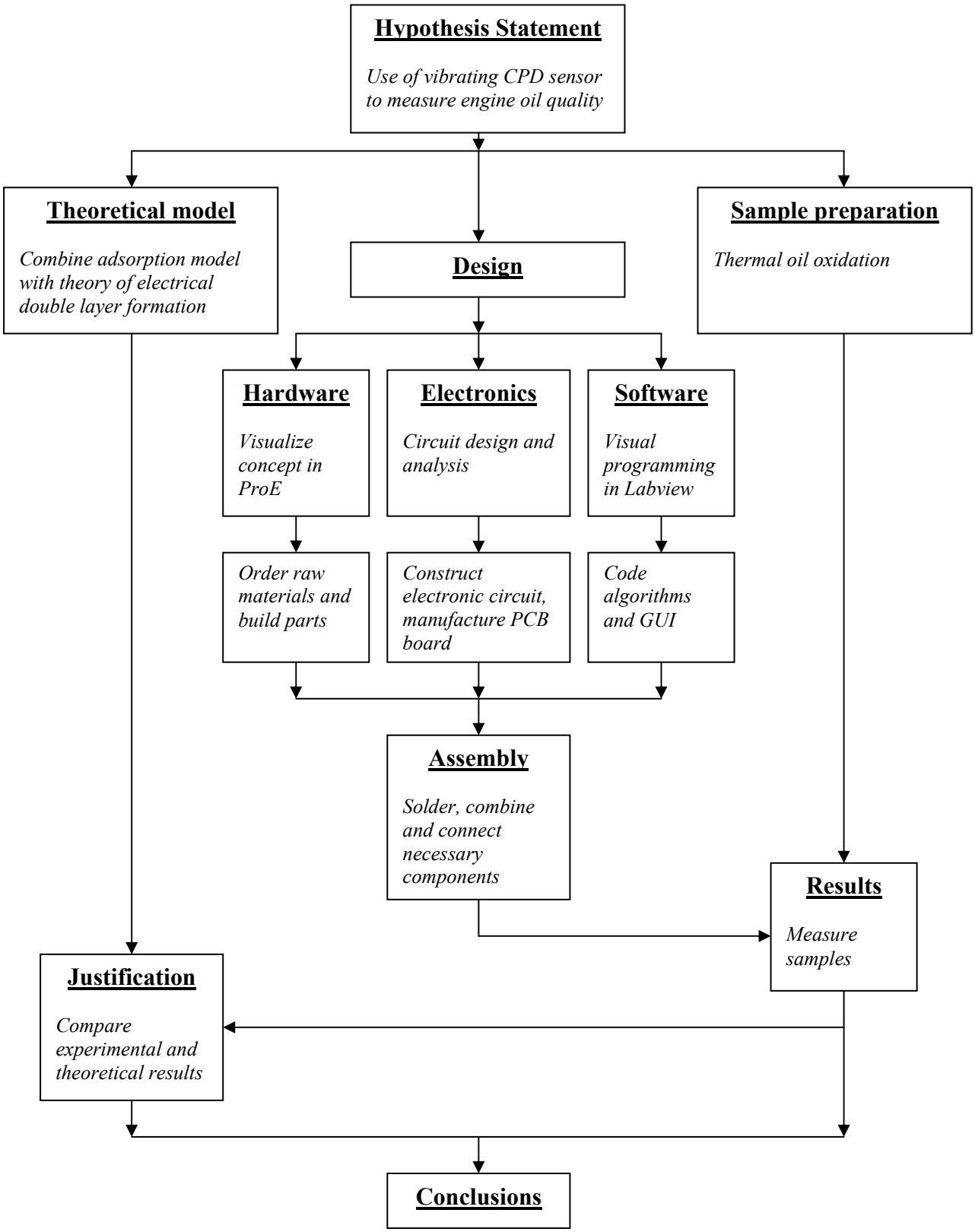

Figure 1-1: Research flow chart

CHAPTER 2

BACKGROUND THEORY

2.1 Surface Potential of Conducting Materials

Surfaces of metals contain electric potentials which prohibit the electrons from leaving the surface. The degree of interaction between an electron and a lattice at the surface of the metal depends on the amount of asymmetry in the lattice and the Fermi level. The only electrons which could leave the surface of a metal are the electrons with enough of energy to overcome the potential barrier on the surface [4].

The surface potential was discovered by Volta and was named after him as the Volta potential. Kelvin utilized this concept in his 1898 paper, the *Contact Electricity of Metals* to relate the charge flow between different metals [5].

2.1.1 Electron Work Function

Electrons in metal even at absolute zero have energies the highest of which is known as the Fermi energy. In order to remove an electron from the metal an energy at least equal to the difference between the surface potential and the Fermi level is needed. The energy required to remove an electron from the Fermi level to outside the metal is called the electronic work function of the metal (Figure 2-1). The surface potential and the electronic work function are related by the equality (2.1).

$$\Psi = \Phi / |e| \tag{2.1}$$

where Φ is the electronic work function of the metal, Ψ is the surface potential, and $|e|$ is the electronic charge [5].

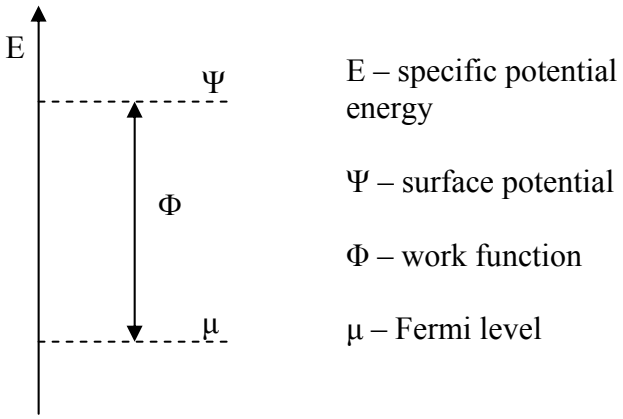

Figure 2-1: Electronic Band Diagram of a Conductor in a vacuum at absolute zero

2.1.2 Physical and Chemical Properties of Surface

Changes in the physical and chemical properties of metal surfaces cause the electronic work function to change. For example, mechanical deformation can influence the work function by changing the degree of interaction between the electrons, dislocations, and the surface. Mechanical deformation creates dislocations and the electronic structure of the dislocation core will affect the Fermi level. This change shifts the Fermi level on the potential energy diagram.

The electronic work function can also change during adsorption. The redistribution of electrons during the bond formation between a free atom or a molecule and a surface dipole layer modifies the work function of the metal. The change of work function can be related to the effective dipole moment of the adsorbate molecules or atoms and the coverage on the surface.

2.2 Contact Potential Difference

As just described the electronic work function is defined as a difference between the electrochemical potential (Fermi level) of the metal and surface potential. In other words it is a work required to remove an electron from the metal and bring it to infinity in vacuum. Figure 2-2 shows a potential diagram for two metals brought into proximity prior to allowing electron flow. The surface potential Ψ is shown in Figure 2-2 as a dashed line.

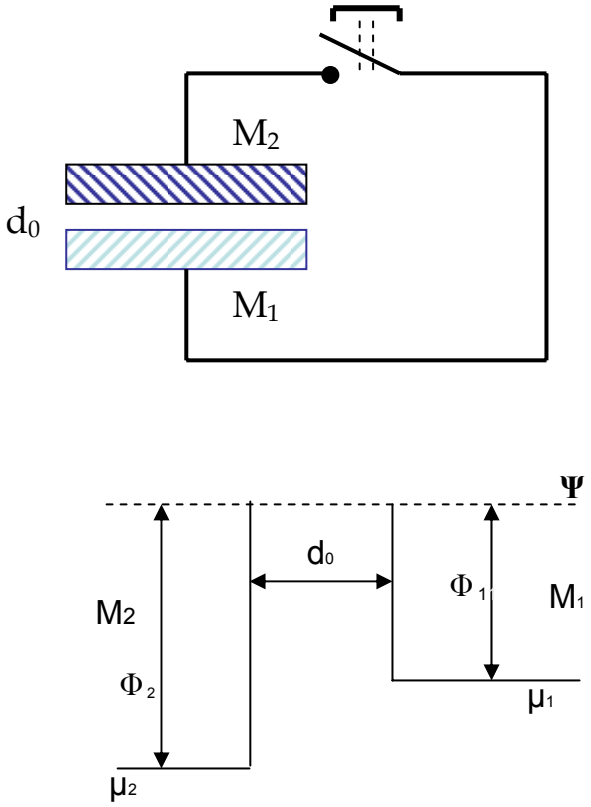

Figure 2-2: Schematic and Potential diagram before equilibrium was settled

Figure 2-2 implies that the work function of the metal on the left is larger than the one of the metal on the right, $\Phi_2 > \Phi_1$. The electrons in the metal with the smaller work function occupy higher energy states, thus they will migrate to the lower states

when those are available. When the switch is opened the electron flow is not possible. That means that each metal is in its own state of equilibrium.

When the switch is closed the electrons from one metal will migrate to the metal with lower work function and the Fermi levels of two metals will equilibrate to a new value [6]. Figure 2-3 shows this state of equilibrium.

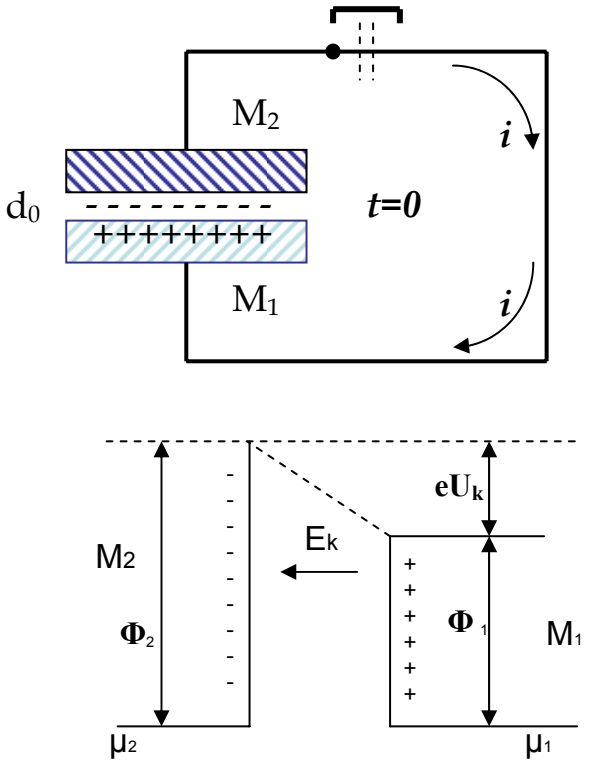

Figure 2-3: Schematic and Potential diagram after equilibrium was settled

Since electrons leave metal M_1 the surface of this metal will be positively charged and the second metal will effectively be negatively charged. Thus an electric field will appear in the gap between the two metals.

Performing the Kirchoff's 2nd Law analysis on the circuit it can be seen that the potential barrier for the electrons moving from right to left is $\Phi_1 + eU_k$ and for the electrons moving from left to right Φ_2.

$$\Phi_1 + eU_k = \Phi_2 \tag{2.2}$$

Rearranging equation (2.2) it is easy to express the potential across the gap between the metals.

$$U_k = \frac{\Phi_2 - \Phi_1}{e} \tag{2.3}$$

The value U_k is called the contact potential difference or CPD between the two metal surfaces.

2.3 The Kelvin Method

The first experiment comprising several metal plates connected in series is known as the *voltaic pile* was devised by Volta in 1799. It was found that when the end plates of Volta's pile were connected to an electroscope the leaves diverged either with positive or negative electricity. Moreover the amount of electricity depended only on the materials of the first and the last plate in the pile [7].

In 1851 Lord Kelvin, by the use of his then newly-invented electrometer, was able to confirm Volta's observations on contact electricity by irrefutable evidence. His experiment used the electrometer to measure the CPD between two metals after they were brought into proximity, electrically connected, and separated afterwards. The electrometer indicated a charge [1]:

$$Q = CU_k \tag{2.4}$$

where C is the capacitance between two metal plates and U_k is the contact potential difference.

2.3.1 The Fundamental Kelvin Probe

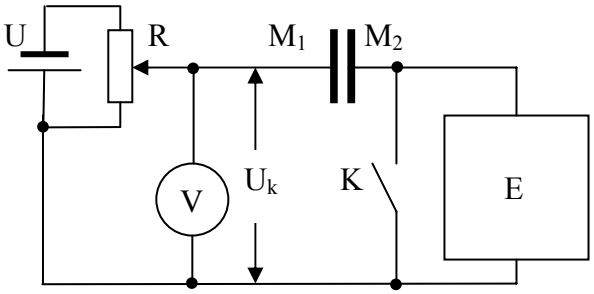

Figure 2-4: The Condenser method modified by Kelvin

An auxiliary DC power source is connected in series with a condenser, which is formed by two plates made of different materials, see Figure 2-4. When the voltage provided by the DC power source U_E is equal to the CPD between metals the electrometer E will show no charge after the switch K is turned in the off position and plates are being moved away from each other.

This situation is described by the equation:

$$Q = C\left(U_k + U_E\right) = 0 \tag{2.5}$$

Equation (2.5) leads to the following equality:

$$U_k = -U_E \tag{2.6}$$

The disadvantage of this method is a difficulty and inconvenience of implementation in a real experimental setup due to the need of manually shifting of one of the plates.

2.3.2 The Vibrating Kelvin Probe

An improvement to the Kelvin Method was done by Zisman who proposed to make one of the plates of the condenser vibrate. The capacitance of such a capacitor periodically changes and an alternating voltage appears across the high-ohmic resistor with the frequency equal to the frequency of the plate vibration due to the existing CPD between the plates. This method allows measuring CPD in a more robust and convenient way. In the literature this method is referred to as the vibrating Kelvin Probe or the Kelvin-Zisman Probe [22-31].

Figure 2-5 shows the schematic diagram of the Kelvin-Zisman probe. It is seen by looking at the equation (2.4) that the charge stored in the capacitor formed by two electrodes is proportional to the CPD. If the electrodes are in close proximity they act as a parallel plate capacitor, and in this case the capacitance can be defined as:

$$C = \varepsilon_r \varepsilon_0 \frac{A}{d_0} \tag{2.7}$$

where ε_r is the dielectric constant of the media between the plates, ε_0 is the permittivity of free space, A is the area of the capacitor, d_0 is the distance between the two plates. In the case of a dynamic capacitor the charge induced by the CPD will create the alternating current across the capacitor. Equation (2.8) describes the current when the CPD (U_k) is either a constant or changes slowly and its derivative is negligible.

$$i = \frac{dQ}{dt} = \frac{d}{dt}\left(CU_k\right) = U_k \frac{dC}{dt} \tag{2.8}$$

Therefore, if the change in capacitance is evoked by sinusoidal oscillation of the one of the plates relative to the other and the voltage drop on R_L is measured, one should get a voltage related to U_k. By changing the voltage of the DC power source we could reach the state when the voltage drop on R_L is zero. This state means that the external DC voltage completely compensates the contact potential difference between the plates of the dynamic capacitor.

The modification suggested by Zisman was taken as a basis for the development of a variety of CPD measurement methods for the use in liquid, ultra-high vacuum, low and high temperature ambients.

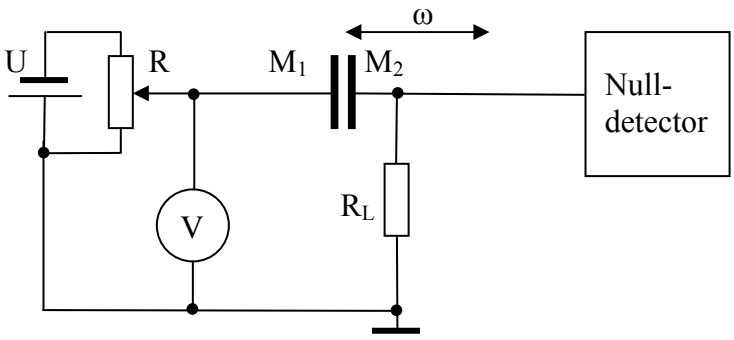

Figure 2-5: The Kelvin-Zisman Method

2.3.3 The Non-Vibrating Kelvin Probe

An alternate way to obtain CPD measurements was proposed by Danyluk and Zharin in 1995 [8]. They suggested using a translation instead of vibration. Relative motion of the surface will result in electrical signals if there is either a geometrical or a chemical change occurring. The signal will reflect the time varying changes in the CPD of the surface, rather than absolute CPD as in the case of the vibrating Kelvin probe.

2.4 Adsorption on Solid Surfaces

2.4.1 Mechanisms of Adsorption

There are several mechanisms which could dominate adsorption onto solid surfaces from an aqueous solution. These mechanisms are strongly affected by the nature of the structural groups on the solid surface along with the molecular structure of the substance being adsorbed and the environment of the aqueous phase. The presence of highly charged sites, the ionic structure of the substance, the electrolyte content, temperature, etc. – together all these factors determine the mechanism by which adsorption occurs, and its efficiency [9].

Ion exchange – Involves replacement of counterions adsorbed onto the surface from the solution by similarly charged surfactant ions. The mechanism of this type of adsorption is shown in Figure 2-6.

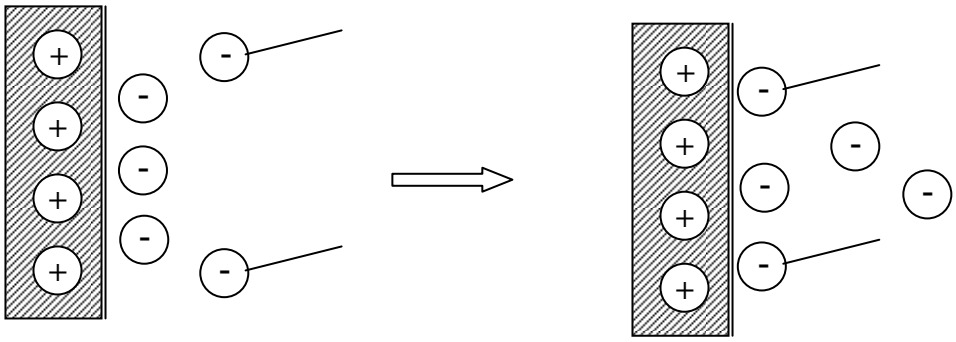

Figure 2-6: Ion Exchange

Ion Pairing – Adsorptions of ions from the liquid solution onto oppositely charged sites unoccupied by counterions (Figure 2-7).

Acid-Base Interaction – The hydrogen bond formation between substrate and adsorbate.

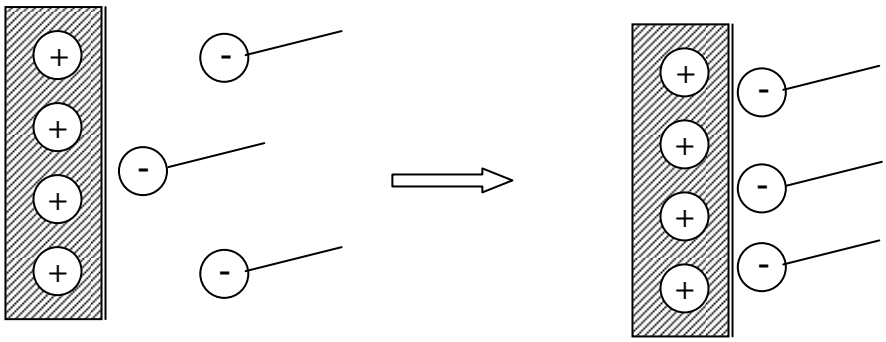

Figure 2-7: Ion Pairing

Adsorption by Polarization of π electrons – Occurs when the adsorbate contains electron-rich aromatic nuclei and the solid adsorbent has strongly positive sites. Attraction between electron-rich aromatic nuclei of the adsorbate and positive sites on the substrate results in adsorption.

Adsorption by Dispersion Forces – Occurs via London-van der Waals dispersion forces acting between adsorbent and adsorbate molecules. Adsorption by this mechanism generally increases with the increase in the molecular weight of the adsorbate and is important only as an independent mechanism, but also as a supplementary mechanism in all other types [10].

Hydrodynamic Bonding – Occurs when the combination of mutual attraction between hydrophobic groups of the solution molecules and their tendency to escape from an aqueous environment becomes large enough to permit them to adsorb onto the solid adsorbent by aggregating their chains [10].

In general, adsorption processes could be subdivided into two subclasses: *chemisorption* and *physisorption*. In the case of chemical adsorption the electron exchange occurs between the adsorbent and the adsorbate. There are two possible consequences of this process – the heat effect due to the ordinary chemical reaction and nonreversible chemical reactions. On the other hand, physisorption is a

completely reversible process. In contrast with chemisorption, during physisorption the adsorbate and the adsorbent interact weakly through van der Waals forces.

2.4.2 The Langmuir Isotherm

If a dilute solution of a surface-active substance is brought in contact with an adsorbing surface of a big area, then extensive adsorption will occur with an attendant reduction in the concentration of the solution. From the analytical data describing the concentration change in the solution as well as knowledge of the total amount of solid and solution equilibrated, it is possible to determine the amount of solute adsorbed per unit weight of adsorbing solid. These types of studies are usually conducted at the constant temperature. Thus, the obtained dependence of total amount of adsorbate adsorbed on the solid surface on the equilibrium concentration is known as the adsorption isotherm.

One of the most popular isotherms and commonly observed in adsorption from the solution is the Langmuir Isotherm, equation (2.9) [10]. This isotherm is one of the easiest to understand theoretically and widely applicable in experimental data processing. The isotherm relates the fractional coverage to the concentration as:

$$\theta = \frac{KC}{KC+1} \tag{2.9}$$

where θ – in the fractional coverage of the surface by the adsorbate;

K – a constant;

C – the concentration of the substance in the liquid phase at adsorption equilibrium;

At infinite dilution $C \to 0$ equation (2.9) becomes (2.10).

$$\theta = KC \tag{2.10}$$

Equation (2.10) shows that θ increases linearly with an initial slope that equals K.

If $KC >> 1$ equation (2.9) becomes:

$$\theta = 1 \tag{2.11}$$

Equation (2.11) indicates that the saturation of the surface with adsorbate is reached.

The Langmuir Isotherm is valid under the following conditions:

1. The adsorbent is homogeneous
2. Both solute and solvent have equal molar surface areas
3. Both surface and bulk phases exhibit ideal behavior
4. The adsorption film is monomolecular

Many experiments have shown this behavior even if these conditions are not satisfied. For example, Beltzer (1992) [11] used this model to describe the adsorption of methyl stearate, stearic, and oleic acids on copper. There is a big class of problems where this type of isotherm does not conform. Adsorption of polymers is the best example of these exceptions. Although this type of problem can be fitted to equation (2.12), which is a re-written Langmuir equation (2.9), but the significance of the constants becomes dubious.

$$m\left(\frac{n}{w}\right) = \frac{(m/b)C}{(m/b)C + 1} \tag{2.12}$$

where m and b are regarded simply as empirical constants;

$\frac{n}{w}$ – the number of moles of solute adsorbed per unit weight of adsorbent.

A method for obtaining the constants could easily be seen by rearranging the equation (2.12) to:

$$C\left(\frac{n}{w}\right) = mC + b \tag{2.13}$$

The rearranged form suggests that the slope of the experimental curve would be equal to m and intercept b.

When the experimental system matches the model, then the values of m and b can be assigned a physical significance:

$$m = \frac{N_A \sigma^0}{A_{sp}} \tag{2.14}$$

where N_A is Avogadro's number;

σ^0 – the area occupied per molecule;

A_{sp} – the specific area of adsorbent.

$$m / b = K \tag{2.15}$$

In the case when the model does not apply, these constants are treated merely as empirical parameters that describe the adsorption isotherm [9].

2.4.3 Effects of Lubricating Films on Work Function

The presence of a lubricating film on the surface of the metal changes the work function of the material surface due to the extreme sensitivity of this parameter to the surface conditions. It is well known that many processes, which occur on the surface, modify the work function of the sample; including adsorption, chemisorption, oxide growth and etc.

Adsorption of molecules of lubricant; chemical interaction between lubricant molecules, the native oxide of the material, and the material itself; formation of an

electrical double layer at the metal-lubricant interface – these are some of the processes which take place on the metal surface in the presence of a lubricant [6].

Considering a lubricating film as a conductive layer upon the surface of the metal, the Debye length for this layer could be calculated. It is known that the electronic work function of a metal surface covered with either an oxide layer or a semiconductor should not change vastly as far as the thickness of the layer is less then Debye length of a dielectric [12].

$$L_D >> h \tag{2.16}$$

where L_D is the Debye length and h is the layer thickness.

The Debye length is defined as a distance from a surface at which a potential of the surface is reduced by e (where e is natural logarithm base) and is determined by:

$$L_D = \frac{\varepsilon_0 kT}{2\pi e^2 n_0} \tag{2.17}$$

where ε_0 is a dielectric constant of material;

k – the Boltzmann constant;

T – the absolute temperature;

n_0 – the concentration of charge carriers;

e – the electronic charge.

According to the Nernst-Einstein equation [13] the dependence of conductivity on the coefficient of diffusion could be shown as:

$$\sigma = \frac{n_0}{k}\frac{e^2}{T}D \tag{2.18}$$

After substituting, rearranging one can get:

$$L_D = \frac{\xi_0}{2\pi}\frac{D}{\sigma} \tag{2.19}$$

Table 2–1 shows the results of calculations for the Debye length for different dielectrics [6]. The calculations show that the Debye length for a dielectric is much bigger than the film thickness achievable during the experiment. Thus we can neglect the change in the lubricant film thickness during the electronic work function measurements.

Oriented dipole molecules at the surface of the metal will contribute to the electron work function as well as to the CPD measurements. In the literature many authors refer to this change as a change in the work function of the surface rather than the work function of the material.

Adsorption processes dramatically change the work function of the material surface due to the redistribution of electrons. During the adsorption bond formation electrons are redistributed between the free atom or molecule and a surface dipole layer.

Previous work of Gottlieb [14] had shown that the surface potential is proportional to the adsorbate surface concentrations, i.e. the number of molecules or atoms per unit area. His work also had shown that the orientation of the molecules does not depend on the area of the surface.

Table 2–1: Debye length for different dielectrics

Substance	Permittivity kl/Vm	Conductivity $Ohm^{-1}m^{-1}$	Diffusion Coefficient m^2/s	Debye length m
Water	81	1E-4	2.43E-9	0.01
Kerosene	24	1E-10	1E-9	5
Transformer oil	2.2	1E-10	1E-9	1
Motor oil	2.2	1E-8	1E-9	0.1
Glycerol	42.4	6.4E-4	1E-10	0.01
Oleic acid	2.46	2E-10	1E-10	0.3
Stearic acid	2.26	4E-13	1E-11	6
Silicone oil	2.2	1E-13	1E-10	10

The Helmholtz equation (2.20) has been used by different researchers to evaluate the magnitude of the potential across the adsorbate with the help of CPD. The equation relates the potential induced by the adsorbed layer on the surface of the metal and adsorbate surface coverage.

$$\Delta(\Delta V) = 4\pi\sigma d \tag{2.20}$$

where σ – is the surface charge density ne;

e – the electronic charge;

d – the dipole distance (separation between "+" and "-" within a polar molecule);

This equation could be recast in terms of dipole moment μ [16]:

$$\Delta(\Delta V) = 4\pi n\mu \tag{2.21}$$

Equation (2.20) as pointed out by Harkins and Fisher (1933) is strictly applicable only to a large scale condenser, where σ and ne is the actual charge density on the condenser plates, and d the distance between plates, not to a dipole in

which charges are attached to molecules, the charges separated by atomic scale distances, not distances between capacitor plates [11].

Gaines (1966) used the modified Helmholtz equation (2.22) in his study of monolayers at liquid-gas interfaces [15]. This equation relates the normal molecular dipole moment and the area of adsorbate molecule to the potential across the monolayer.

$$\Delta(\Delta V) = \frac{\mu_N}{\varepsilon_r \varepsilon_0 A_M} \tag{2.22}$$

where μ_N – is the normal component of the molecular dipole moment;

ε_r – the permittivity of substance;

ε_0 – the permittivity of free space;

A_M – the area of one molecule.

Korach, Streator and Danyluk (2001) [17] were able to use this model to describe the surface potential change on the rotating magnetic disk in the presence of lubricant. In their experiment they used the non-vibrating CPD to study film thickness distribution on the rotating magnetic disk.

Although the Helmholtz equation is not directly applicable in general it is useful in the sense that it approximately relates $\Delta(\Delta V)$ to molecular orientation, as well as to surface coverage. The contact potential is proportional to the surface concentration, but the proportionality is not related in a simple way to the normal or any other projections of the dipole moment.

If only a single surface active substance is present, the surface potential is proportional to the number of molecules per unit area and the normal component of the molecular dipole moment [18]. Although ΔV may be proportional to the surface

density of adsorbed dipoles on the metal, the contact potential measurement can not by itself determine the actual surface density. This must be done by independent method such as radiolabeling [11].

However, $\Delta(\Delta V)$ can also be related to the fractional surface coverage θ:

$$\Delta(\Delta V) = k\theta \tag{2.23}$$

where k – proportionality coefficient.

The dependence of fractional coverage θ on the bulk solution concentration is a function of the adsorption isotherm of the particular experiment. Therefore the relationship of the relative CPD output voltage to a particular isotherm would be expected to be the same as θ.

2.5 Oil Sensors Classification

Oil analysis is a vast field comprised of hundreds of individual tests that provide meaningful benefit by assessing one or more properties of a lubricant or machine. Many of the tests are performed on new types of oil during research and development. The lubricant's chemical, physical, or lubricating properties are validated for quality control purposes and product performance classification.

The main focus of oil testing techniques is to determine changes in oil properties. The objective of these techniques is considerably different from new oil analysis. The objective for used oil testing is either to assess the quality of the oil that is currently being used in machinery, engine, or to evaluate the machine condition itself. The lubricant is an exceptionally valuable source of information about wear and corrosion happening in the machine.

Three big classes of oil analysis are shown on Figure 2-8. The fluid properties analysis gives an assessment of the chemical, physical, and additive properties of oil. Among the techniques that analyze fluid properties tests like the viscosity measurement, the Acid Number and the Base Number tests may be emphasized.

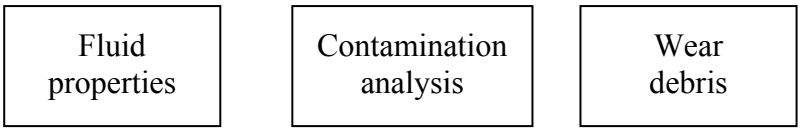

Figure 2-8: Classes of oil analysis

Viscosity affects equipment operation, friction losses and the oil film thickness in bearings. Applied to industrial oils, the total acid number is a measure of total acid concentration of the oil. With the increase of acid number oil becomes highly corrosive attacking bearing materials and other metal surfaces. The base number test measures the reserve alkalinity of an oil. Engine oils are equipped with additives that provide reserve alkalinity to neutralize the acids that are generated during combustion. The lack of ability to neutralize the acids will cause corrosion to increase [19].

The second class of oil tests deals with contaminants which are present in the bulk oil. By definition a contaminant is a foreign substance that enters the system from the environment or is generated internally and its presense in general is not desirable. Contamination compromises machine reliability and promotes lubricant failure. Fourier Transform Infrared (FTIR) spectroscopy, Elemental spectroscopy, Conductivity Test [20], the Dielectric constant measuremets [21] are the main methods for contaminant analysis in the oil industry.

When parts inside the machine wear, debris are generated. Monitoring and analysing the generated debris enables technologists to detect and evaluate abnormal conditions so that effective maintenance decisions can be made and implemented. The

Particle Count test, the Ferrous Density and the Analytical Ferrography test are the tests that are commonly used for wear assessment.

On the other hand, oil analysis sensors may belong to two different families – either online or offline sensors. The convenience of taking samples in situ together with the rapid response from the sensor is an advantage of the online sensors used in engines and manufacturing equipment. Contemporary online sensors lose to their offline competitors in the quality of analysis. FTIR analysis of motor oil gives much broader analysis than any of the online sensors by giving the elemental spectrum. The online sensor installed in the engine gives a coarse estimation of the processes happening in the lubricating system and in the machine itself. It is commonly recommended for the industrial machinery and engines to evaluate the lubricant properties offline on the regular basis but still have online sensor for a rapid response in the case of emergency. In today's market there are many companies offering online as well as offline sensors and systems for oil monitoring and analysis, among them Lubrigard, Delphi, Foster Miller, Gas Tops-Metalscan and others.

All oil testing techniques could be classified as presented in Figure 2-9. All the methods mentioned here are well developed and widely used in the industry, automobile and truck fleets, except the methods based on the adsorption properties of oils. These methods are still not well understood and not used as extensively as others.

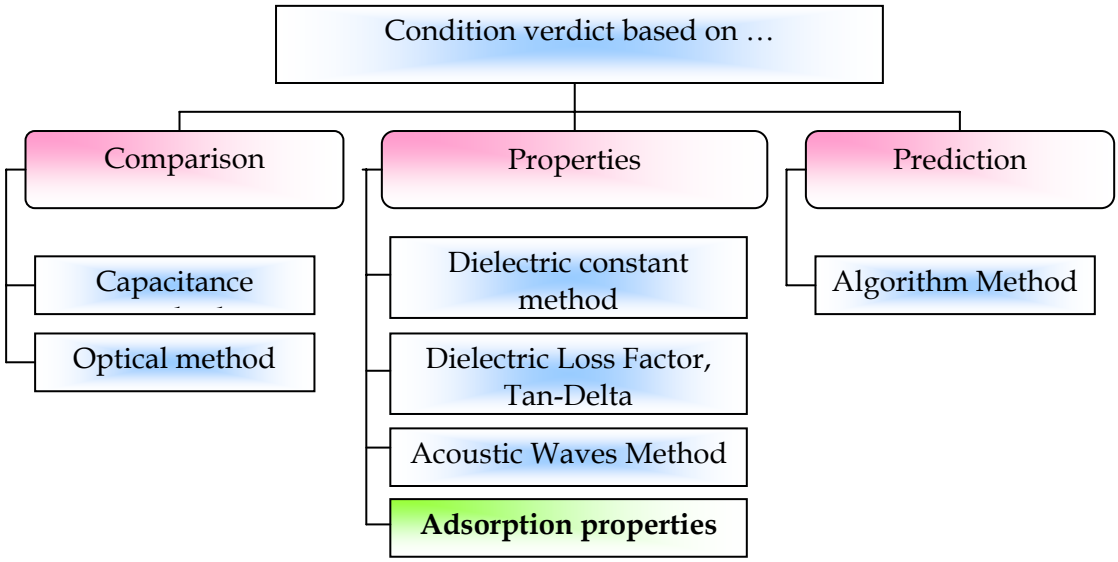

Figure 2-9: Classification of Oil Testing Techniques

CHAPTER 3

EXPERIMENTAL

3.1 Overall System Design

The schematic diagram of a system utilizing the Chemical Degradation Oil Sensor (CDOS) is shown in Figure 3-1.

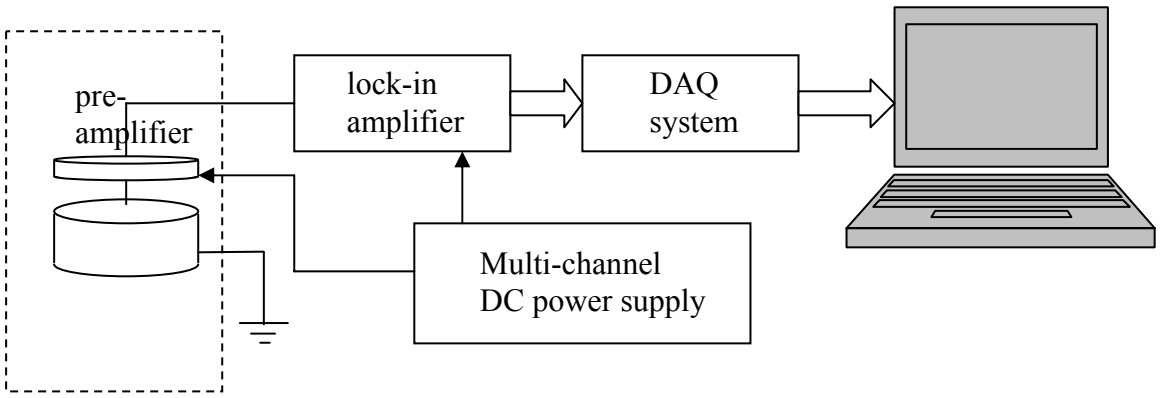

Figure 3-1: Schematic Diagram of CDOS system

The part of the diagram outlined with a dashed rectangle constitutes the CDOS sensor. The systems functions as follows: the signal generated by the CDOS sensor is amplified and fed into a phase-sensitive rectifier which allows the detection of small currents (in the order of hundreds of picoamps) over the background of the noise generated by the electronics and external hum. Further the signal from the rectifier is digitized by the data acquisition system and results are stored in the memory of the computer.

An oil sample is placed into the sensor manually, see Chapter 3.5. This feature deters the current sensor design from being implemented in online application but it can still be used in an offline portable or static system. A photograph of the experimental setup is shown in Figure 3-2.

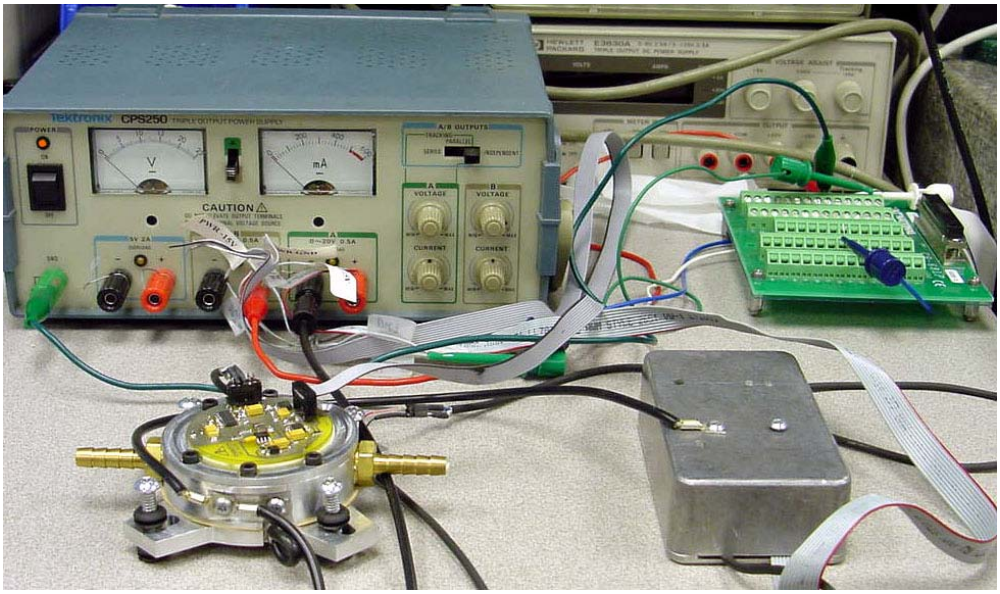

Figure 3-2: Photograph of the experimental setup

In order to design a robust and a reliable experimental system utilizing the CDOS type of sensor the following aspects should be taken into consideration:

i) Stable low noise multi-channel power supply;

ii) Good grounding of the sensor and the equipment;

iii) Low speed DAQ system with logging capabilities.

The equipment used in the experimental setup is listed in the Table 3–1. The table quotes the type of the equipment and its main electrical characteristics.

Table 3–1: The equipment list for the experimental setup

Equipment	Model	Characteristics
DC POWER SUPPLY	Tektronix CPS250	Triple output power supply, 5V - 2A, 2x0~20V – 0.5A
DAQ SYSTEM	National Instruments PCI NI-6034E	16 analog inputs, 200 kS/s, 12 or 16-bit resolution
PERSONAL COMPUTER	DELL Intel Pentium 4(R)	1.70GHz, 512Mb, Windows XP , Service pack 2

3.2 Mechanical Design of the CDOS Sensor

A number of considerations were taken into account at the design stage of the sensor. The sensor should be easy to operate when changing oil samples, accurately machined, utilize piezo vibrator, have a possibility to be used in online tests, have an appropriate sealing to operate with lubricants.

The schematic diagram of the cross-section of the sensor system is shown in Figure 3-3.

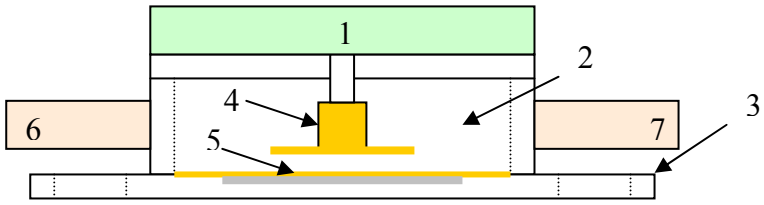

Figure 3-3: The cross-section of the CDOS sensor.
1 – preamplifier compartment; 2 – lubricant compartment; 3 – base lid with fastening holes; 4 – active electrode; 5 – passive piezo vibrating electrode; 6,7 – optional lubricants inlet and outlet.

All metal parts of the sensor were machined from Alloy 2011 aluminum. As shown in Figure 3-3 the sensor consists of a preamplifier compartment, containing the

circuit board of the preamp and serving as an electrical shield, and a lubricant compartment (Figure 3-4-a) that serves as a lubricant container and is properly sealed with a help of gaskets made of neoprene rubber capable of resisting to lubricants and high temperatures. The bottom of the lubricant compartment contains a vibrating piezo plate which serves as a passive electrode. A commercially available piezo buzzer CEB-44D06 was used as the vibrating plate. The active electrode was machined into the T-shape to reduce the stray capacitance and increase the effective area of the probe (see Figure 3-4-b). Brass was used as a material for the active electrode. The bottom part of the sensor contains four fastening holes in order to fix the sensor on the experimental setup. The lubricant inlet and outlet are foreseen for possible online tests.

A photograph of the assembled CDOS sensor is shown in Figure 3-5.

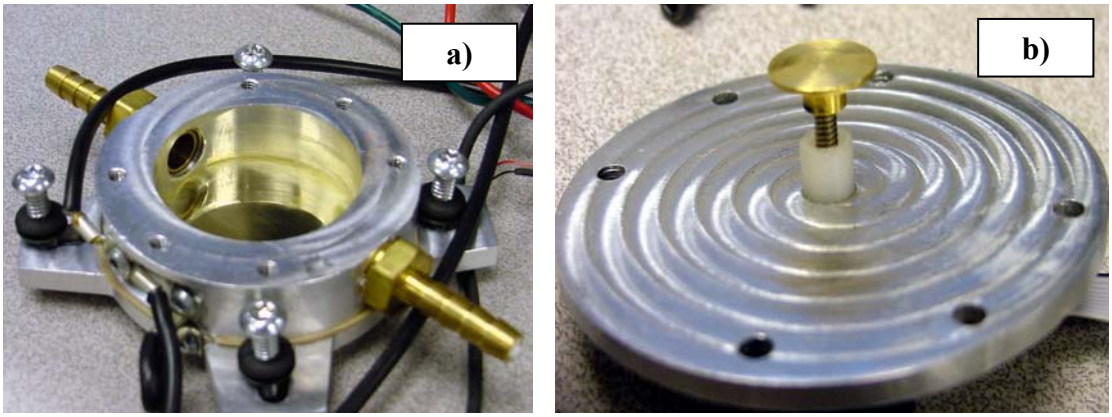

Figure 3-4: Developed CDOS sensor – Opened.
a) the lubricant compartment
b) the T-shape active electrode

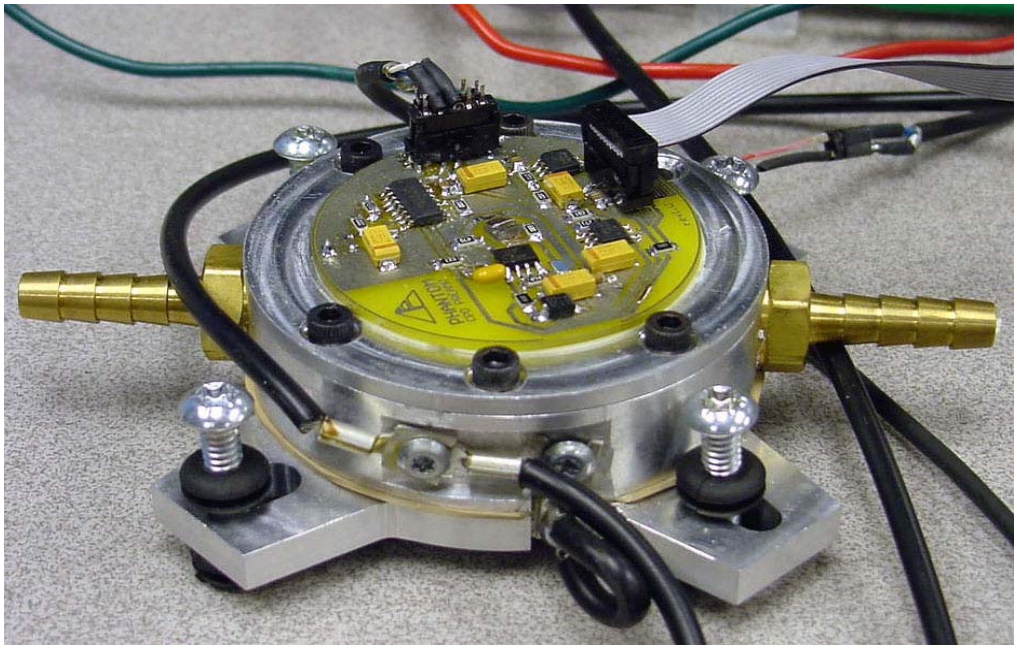

Figure 3-5: Photograph of the developed CDOS sensor

3.3 Electronic Circuit Design

An analog circuit for the preamplifier and amplifier of the experimental setup was built using a novel toner transfer technique. This technique is harmless and not hazardous as the pre-synthesized photo boards. Ferric Chloride was used to etch the circuit boards.

As shown in Figure 3-1 the system employs two electronic units. They are the preamplifier board and the lock-in amplifier.

3.3.1 Preamplifier

The preamplifier board is responsible for the following:

i) amplification of a weak input signal

ii) noise reduction using simple analog filtration

iii) bias application to the active electrode plate

The schematic diagram of the preamplifier board is shown in Figure 3-6. The U3 is an ultra low bias current OPA129 operational amplifier. In the circuit it is used as an ultra sensitive current to voltage converter converting the current induced by CPD into measurable alternating voltage. The gain of this cascade was calculated to be $G=4.01*10^{10}$ at 250Hz (see Appendix III). At the output of the cascade the noise absolute value is not greater than 1mV. Further signal from U3 passes through the RC low band filter and follows to the buffer amplifier U1A.

The "Phantom ground" method was used in the circuit to apply bias to the active electrode. This method artificially shifts the ground potential of the first amplifying stage to the level needed. Due to the inverting circuit behavior of the first stage the potential of the active electrode connected to the inverting input of the operational amplifier U3 will follow the potential of the voltage shift. The following ICs participate in the formation of the "phantom ground" effect – U2, U4, and U1B. Integrated circuits U2 and U4 form ±6V potentials with respect to the "phantom ground" which are used for powering the amplifier U3. The operational amplifier U1B serves as a buffer for the input bias voltage.

In Figure 3-6 the *CPD_input* wire trace represents the circuit input, namely the active electrode connection. The *CPD_feedback* is a bias voltage input, or a compensation bias input. *CPD_output* is the output of the probe which further is processed by lock-in amplifier.

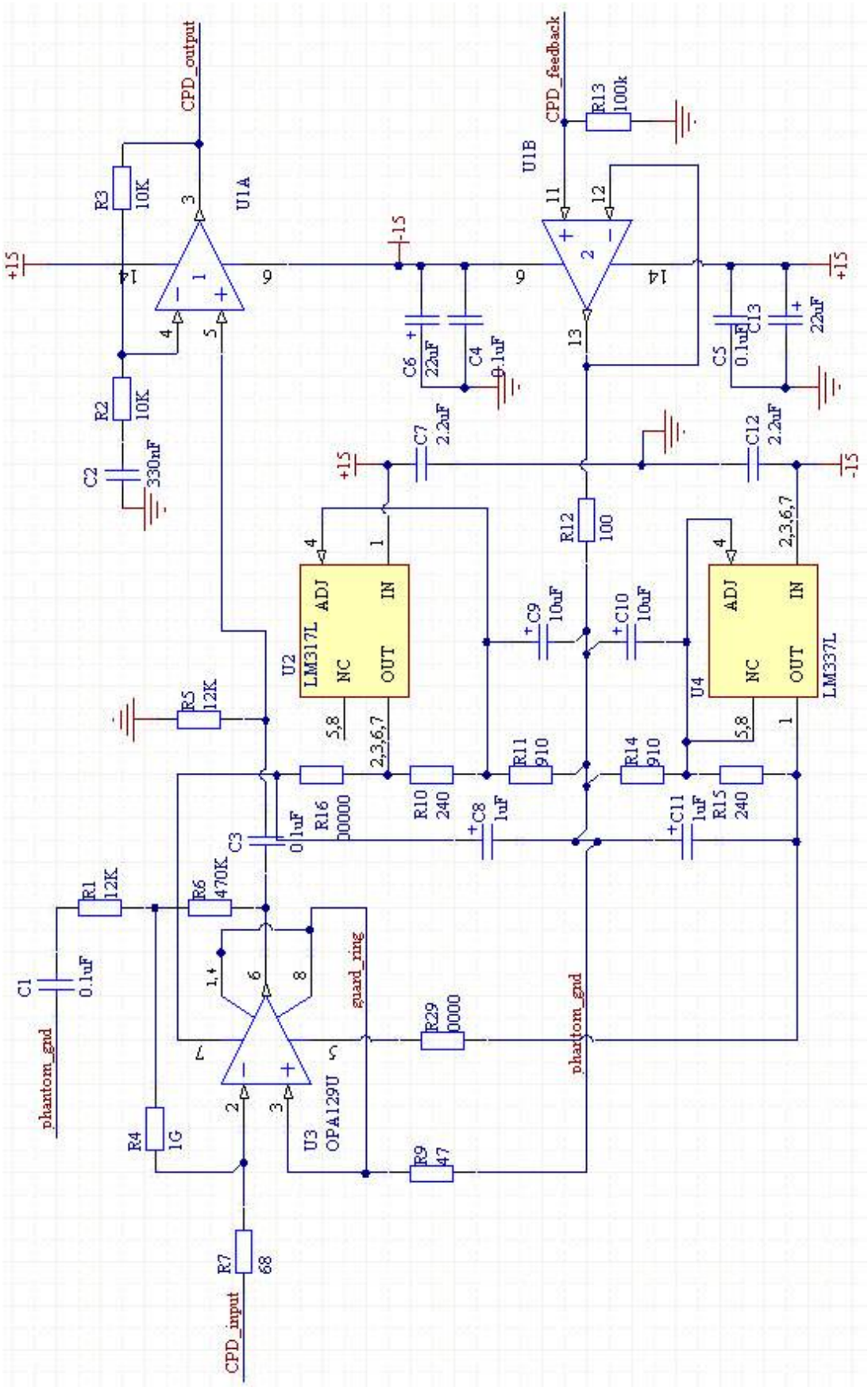

Figure 3-6: Circuit diagram of the preamplifier board

3.3.2 Phase-sensitive Rectifier

A lock-in amplifier or a phase-sensitive rectifier is needed with these features:

i) Detection of noisy signals

ii) Detection of signals superposed with other signals having a greater amplitude but different frequency

iii) Detection of harmonic signals superposed with phase shifted signals with the same frequency

On the other hand, the circuit design requirements listed below will guarantee a stable and correct measurement of the signal, when implementing lock-in techniques.

i) Rejection ability to the power supply instabilities

ii) Stability to temperature change

iii) Stability of the quadrature module

The main application of this technique in the CDOS sensor experimental setup is a phase rectification of the signal from the sensor. In order to obtain correct measurements several precautions should be taken, among them are a stable power supply, and phase tuning.

The lock-in amplifier circuit was developed in the research lab by Dr. Zharin. The developed circuit could be represented schematically as shown in Figure 3-7.

As shown in Figure 3-7, the input reference signal is used to form a square wave signal with the help of Schmidt-Trigger circuit. The waveform has the same duty cycle, frequency, and phase as the input signal. This square waveform is fed into

a switching rectifier to form two unipolar signals. The advantage of using two unipolar signals versus only one is the bigger sensitivity of the circuit. Two formed signals are processed by the differential integrator/inverter and the constant level appears at the output of the circuit.

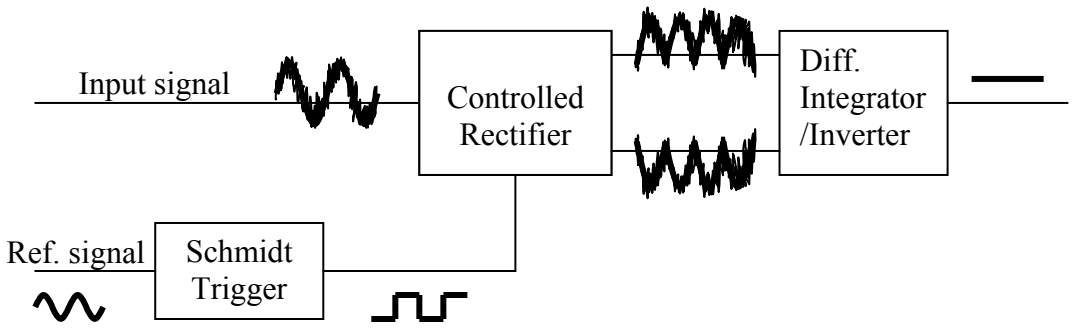

Figure 3-7: Schematic diagram of the phase sensitive rectifier

As the phase-sensitive rectifier uses the external harmonic signal as a reference signal, it is very important that it is does not distort the input reference signal when forming the square replica of it. This means that the duty cycle of the replica signal should be exactly the same as the original harmonic signal.

This constant potential is supplied to the bias level input of the CDOS sensor (see Chapter 3.3.1). Because of the inverted character of the signal, the amplitude of the signal generated by the CDOS sensor will reduce so will the input of the lock-in amplifier. It is easy to see that the voltage generated by the lock-in amplifier will not change when the CPD potential between the plates of the capacitor is fully compensated; this means that the CDOS sensor will give a nil output. The lock-in amplifier will "remember" the last potential before the compensated state, which will be equal to the CPD.

The time constant of the lock-in amplifier was chosen to be 2 seconds. All the electronics was tuned to the operating frequency 250Hz. A photograph of the lock-in amplifier is shown in Figure 3-8.

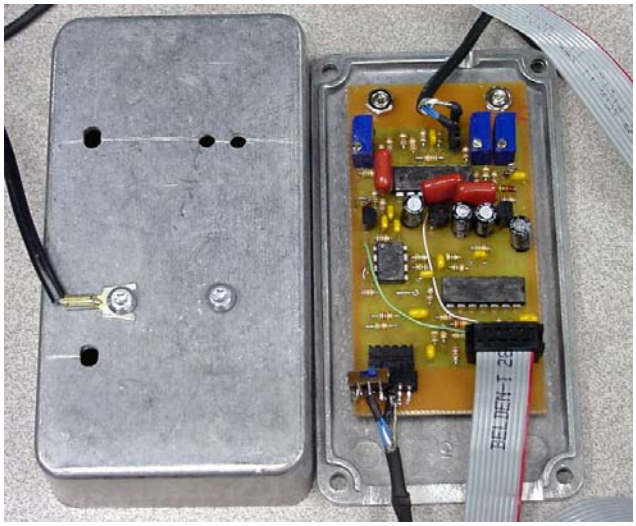

Figure 3-8: Photograph of the Lock-In Amplifier developed by Zharin

3.4 Data Acquisition System

A low-speed data acquisition (DAQ) system was utilized to record raw data from the Chemical Degradation Oil Sensor after the preprocessing was done by the analog circuits described in Chapter 3.3. The DAQ system is PC based and consists of a 16-bit National Instruments DAQ PCI-6034E board which has a capability of receiving up to 16 differential or 32 single-referenced signals in the range of ±10V. The board has a data acquisition rate up to 200KS/s. The National Instruments connector block CB-68LP was used for the physical connections between the DAQ and the CDOS sensor setup.

Labview 7.1 was used to program the acquisition for the experiment. The graphic user interface (GUI) specifically designed for the experiment is shown in Figure 3-9.

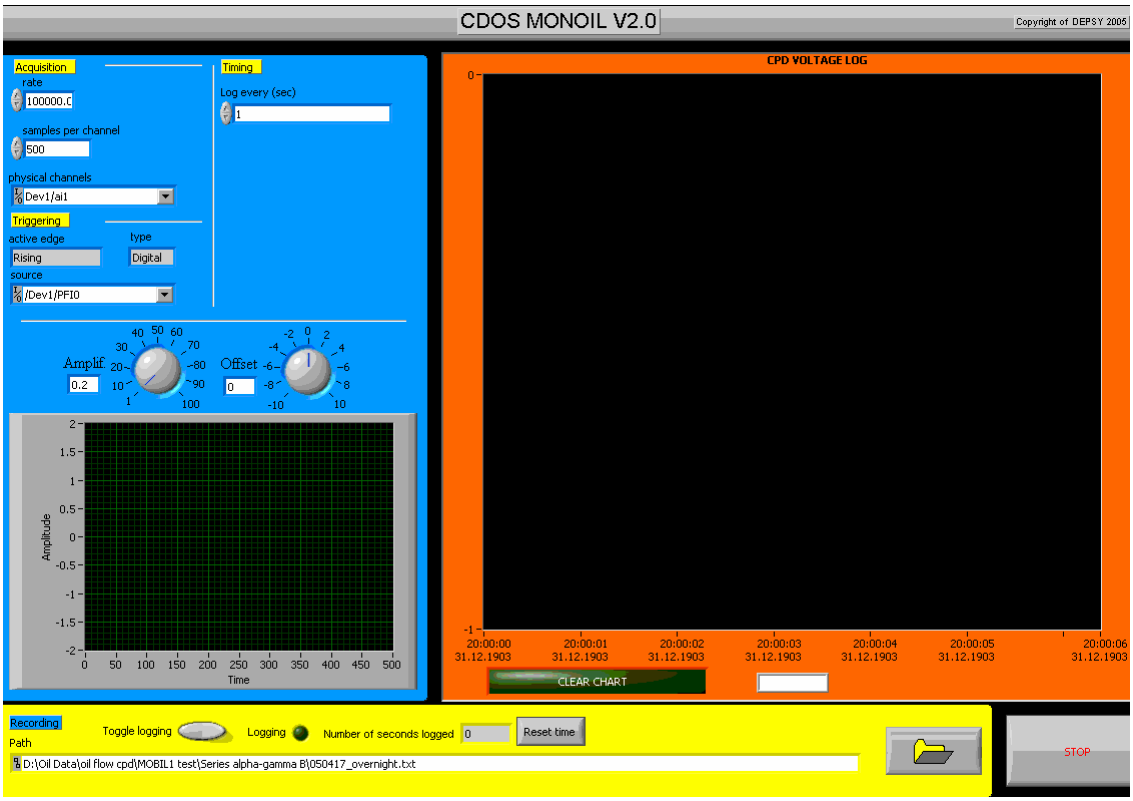

Figure 3-9: Screenshot of the Labview virtual instrument GUI

As it can be seen from Figure 3-9 the designed virtual instrument allows the operator to set appropriate settings for the acquisition. The sampling rate, the number of samples, the physical channel, and different trigger settings can be set using the GUI of the virtual instrument. The user is allowed to select the interval in seconds between data sampling and allows him to control the frequency of data logging into the file and the screen. The virtual instrument is also programmed to play a sound every 10 minutes of acquisition to coarsely inform the operator about elapsed time.

The GUI retains a big display for the logged sensor data and a small secondary window which could be used for different purposes. In the experiment this display was used to monitor the quality of the phase tuning in the lock-in amplifier.

The details of the developed virtual instrument diagram are presented in Appendix I.

3.5 Experimental Test Procedure

Figure 3-10 shows the flow chart for the experimental procedure for taking measurements using CDOS sensor and the experimental setup. The highlighted part of the procedure, “Sample Change” stage, is extremely important because it determines the repeatability of the experiment and will be discussed in detail later in this chapter.

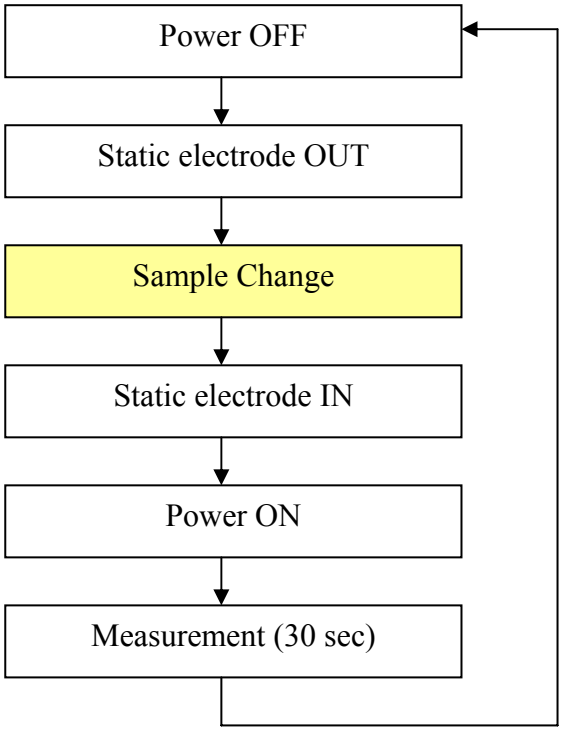

Figure 3-10: Flow chart of the experimental procedure

In order to take a new measurement the system should be powered off. The static electrode (see Figure 3-4-b) should be separated from the sensor. Sample change is the next step that should be taken. After that the static electrode should be placed back in the system and power be turned on. The measurement could be taken afterwards. The interval length during which data is being recorded is equal to thirty seconds.

As shown in Figure 3-11 the sample is located on the bottom surface of the static electrode and isolated with an air gap from the vibrating electrode. The procedure of changing the sample is shown in Figure 3-12. The thickness of the applied film was roughly estimated to be 200 microns.

No chemicals were used during the sample change. It was noticed that the cleaning with petroleum ether and methanol introduced poor repeatability into the experiment. Besides, no use of chemicals approximates the online behavior of the sensor.

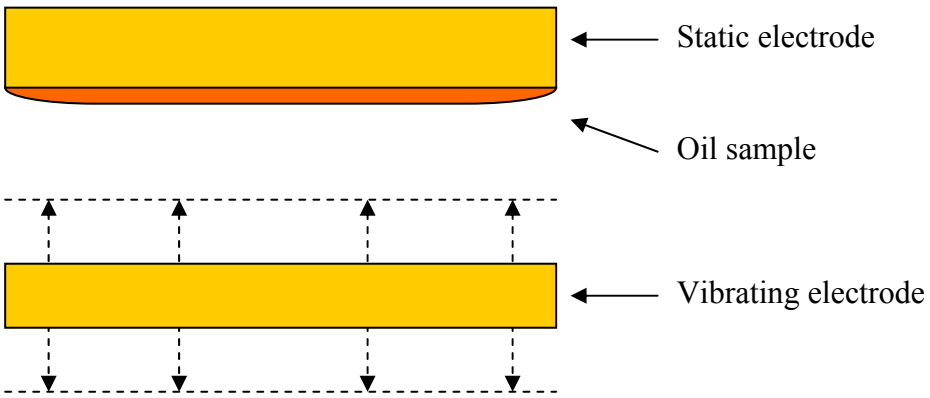

Figure 3-11: Sample location in the CDOS sensor

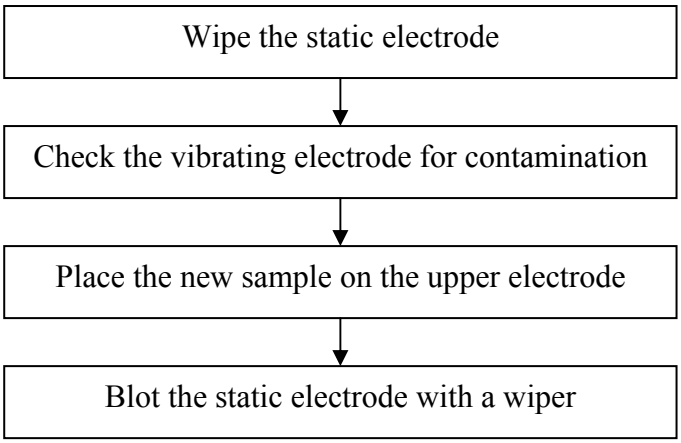

Figure 3-12: Procedure for the sample change

3.6 Samples Preparation

In order to show that the developed sensor is capable of detecting the level of oxidation in engine oil, several samples were prepared in the lab. The thermal aging method was used to prepare the samples.

MOBIL1 10W30 fully synthetic oil was used for the experiments. 100ml of the oil was placed into the flask and was aged at 180^0C on the hotplate. The setup used to age the synthetic oil is shown in Figure 3-13.

The oil samples were taken at different time intervals. Table 3-2 shows the samples that were prepared by the method described above.

Figure 3-13: Setup for the thermal aging of oil

Table 3–2: Synthetic oil samples prepared by the intentional oxidation

#	Sample Alias	Aging time, min
1	F1	0
2	F2	15
3	F3	30
4	F4	60
5	F5	120
6	F6	240
7	F7	380
8	F8	1440

3.7 Design of Experiment

In order to improve the reliability of the experimental data the tests were randomized. Each sample was run a total of six times on the CDOS sensor experimental setup. Table 3-3 shows the DOE for the experiment. The test sequence coincides with the row-wise order from left to right.

The experiments were randomized within each row of the table. This approach allows us to observe a drift that could present in the system and accounts for it in further data processing.

Table 3–3: The DOE for the thermally aged oil experiment.

	1	2	3	4	5	6	7	8
1	F4	F2	F6	F1	F3	F7	F5	F8
2	F1	F3	F7	F2	F5	F8	F6	F4
3	F7	F4	F1	F5	F8	F2	F3	F6
4	F2	F5	F8	F6	F1	F4	F3	F7
5	F7	F2	F5	F3	F1	F6	F8	F4
6	F8	F2	F4	F6	F5	F7	F3	F1

CHAPTER 4

RESULTS

This chapter will summarize the experimental results. The focus of the experiment was to gain an understanding of the relationship between the output of the CDOS sensor and the degree of oxidation of the oil. It is proposed that these results are due to the surface potential change as well as the changes in the electrical double layer formed upon the surface.

4.1 Thermally Aged Oil Experiment

A total of eight samples of intentionally oxidized synthetic MOBIL 1 oil were run on the CDOS experimental setup. The experimental procedure was carried out according to the one described in Chapter 3. As it was already pointed out, the tests were intentionally randomized within the row of the DOE matrix. For simplicity every line of the DOE matrix will be called an *experimental batch* for the rest of this chapter.

When plotting the data it is reasonable to plot every experimental batch with the same abscissa. All experiments were run in one batch; there were no delays in between experiments. That justifies the plotting method mentioned above. After the data was plotted it was possible to calculate and further subtract the experimental system drift.

The raw experimental data plotted by the method described above is shown in Figure 4-1. In addition, the experimental data grouped by the sample type is shown in Figure 4-2.

It can be seen from Figure 4-1 that the system has a noticeable drift over time. First several experimental batches show a bigger voltage response than the previous ones. This behavior could be explained as either the circuit instability or the surface condition change. The last aspect is more important because, as was shown in the preceding chapters, the CPD technique is extremely sensitive to the chemistry of the sample and the degree of interaction between a sample and a sampling surface. Some of these interactions could be slow reactions. The reactions could also have a permanent effect on the surface (e.g. corrosion) that would result in system drift.

A visual observation of the surface in between the tests helped to conclude that there is an obvious change in surface condition due to corrosion. The surface of the electrode changed from shiny to dull after a long presence in the oil.

In order to subtract the drift from the experimental data the mean value of the experimental batch was calculated. Voltage deflections from the mean curve were calculated afterwards for each of the eight samples. The systems drift along with the experimental batches is shown in Figure 4-3.

Subtracting the systems drift from the all experimental data curves will result in the experimental data which look as shown in Figure 4-4 and Figure 4-5. This additional procedure of subtracting the system drift helped reduce the standard deviation of the experimental data by 17%.

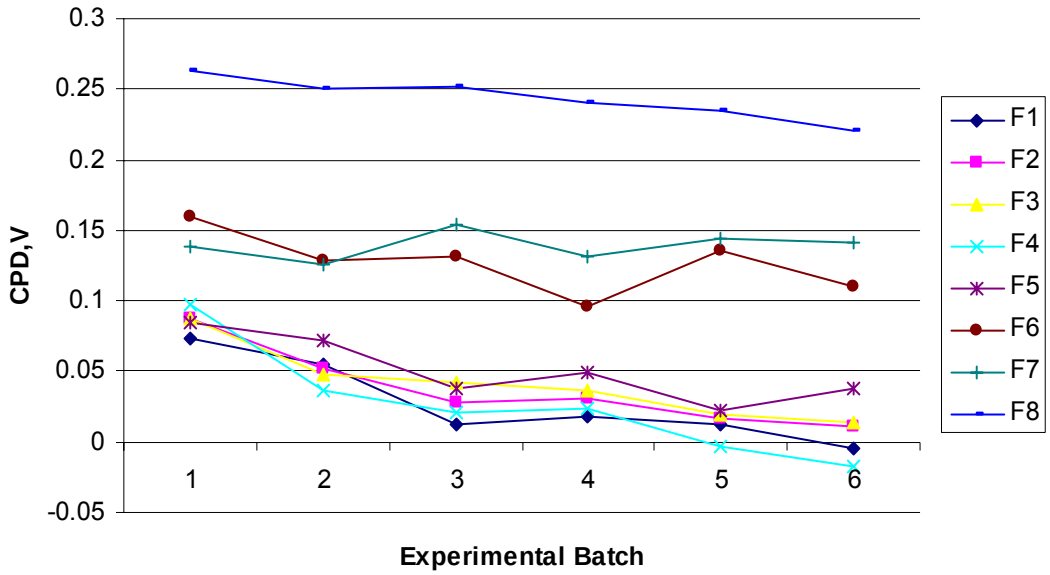

Figure 4-1: Raw experimental data grouped by the experimental batches

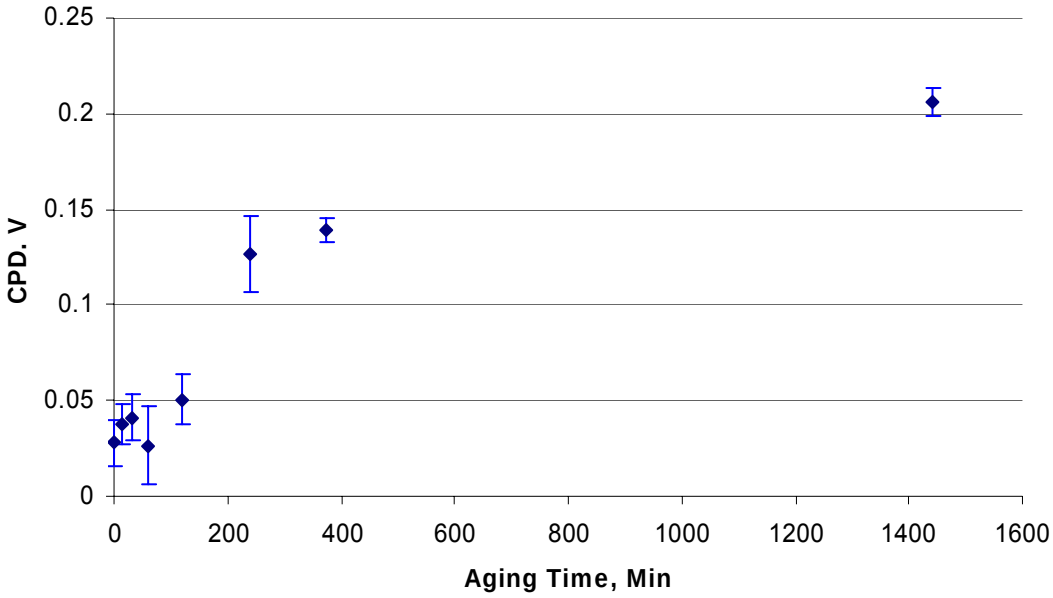

Figure 4-2: Raw CDOS sensor output versus aging time

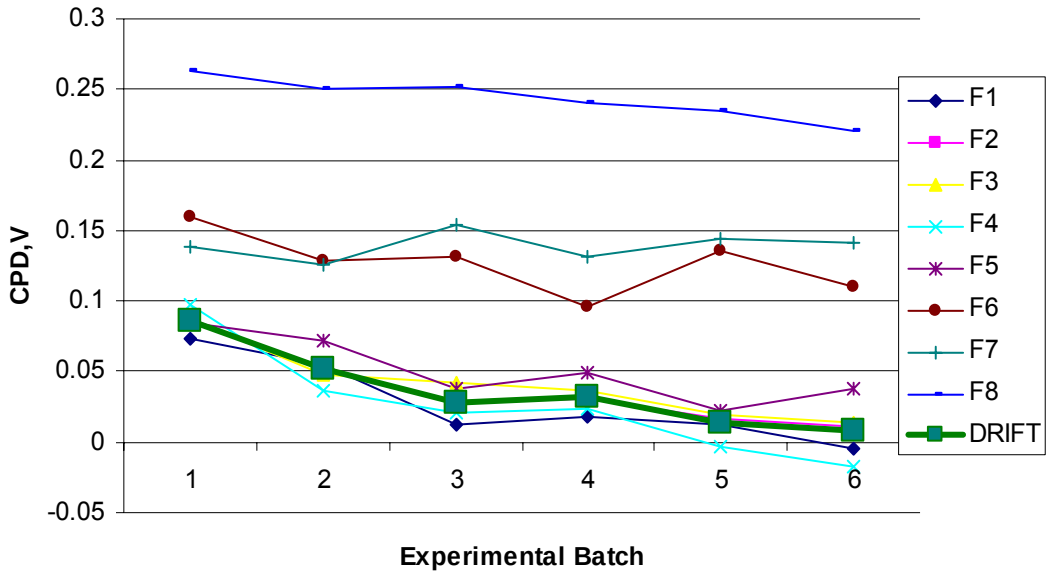

Figure 4-3: Experimental systems drift with time

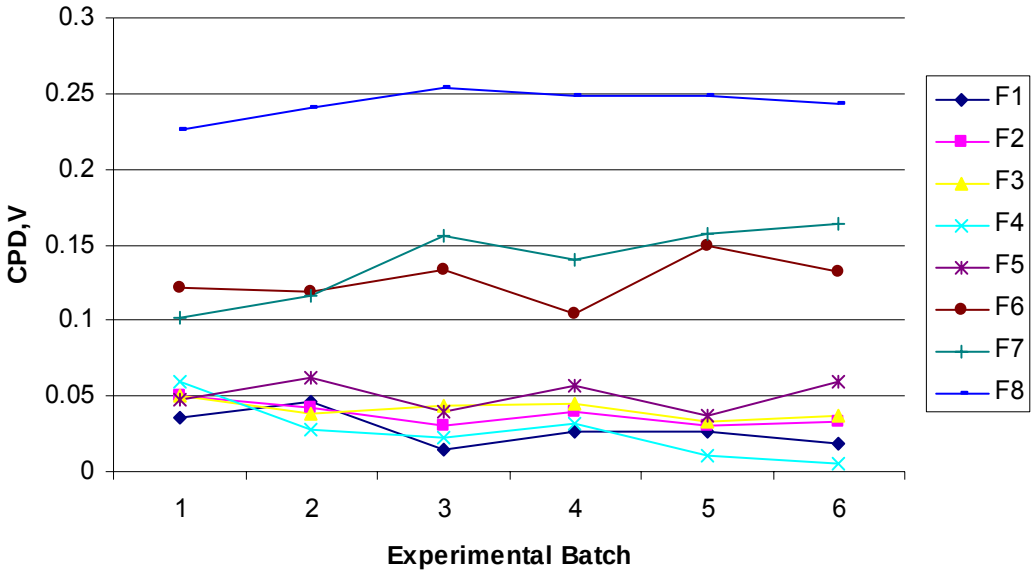

Figure 4-4: Processed experimental data grouped by the experimental batches

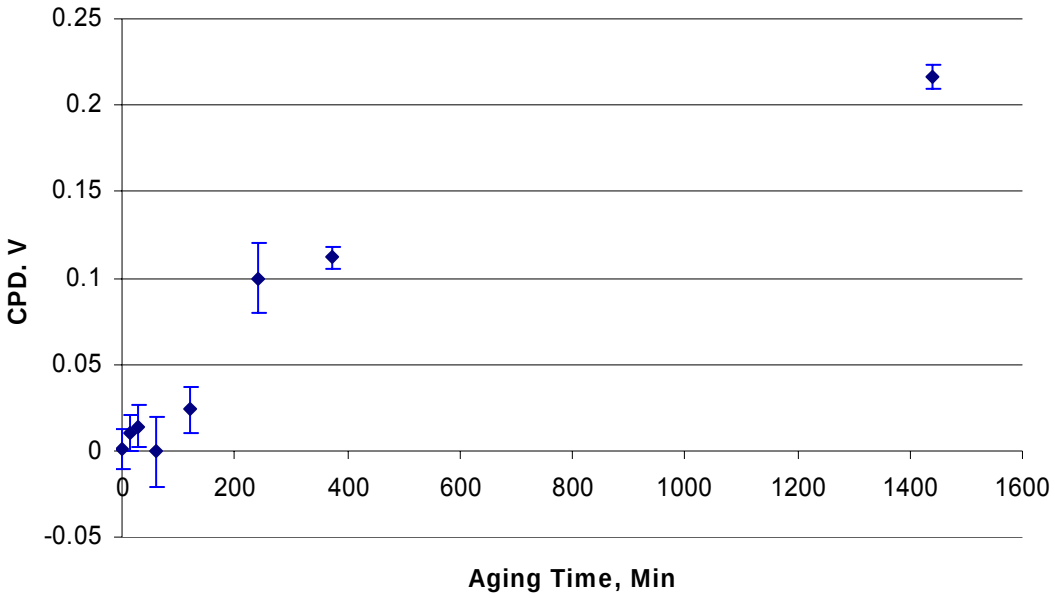

Figure 4-5: Processed CDOS sensor output versus aging time

CHAPTER 5

DISCUSSION

This chapter focuses on the explanations of the sensor response curves presented in Chapter 4. The theoretical model will be presented as a comparison to the data. The applicability of this model to the CDOS sensor output will be discussed.

5.1 Depletion of Antioxidants and Detergents

Lubricant antioxidants enhance thermal stability, improve lubricant performance, and reduce sludge formation, extending the useful life of lubricants in virtually any application. They reduce thickening and inhibit acid formation in a variety of applications, including engine oils, automatic transmission fluids, 2-cycle oil and paper mill oil, as well as compressor oil and gear, and hydraulic oils [19]. On the other hand, detergents are used to clean up the by product of oxidized oil which occurs when antioxidants can not neutralize the acids effectively by creating a chemical reaction with sludge, and varnish precursors so to neutralize them and keep them soluble.

The amount of antioxidants along with detergents in the bulk oil is depleted over time and degradation products increase not only with the increase in temperature, but also with the increases in mechanical agitation or turbulence and contamination – air, water, metallic particles and dust.

Monitoring the amount of antioxidants and detergents in the oil is a very important part of maintenance in critical machinery. The ability to analyze this parameter gives the opportunity to respond in a prompt manner to the changes in lubricating conditions. It serves as a preventing means of increasing the machine useful life and saves on repair of the machine.

Taking a closer look at the experimental data (see Figure 5-1 and Figure 5-2) it is easy to notice a local maximum and a minimum at the beginning of the thermal aging process. This interval of the experiment conforms to the start of the thermal aging of the oil. At that time antioxidants and detergents present in the oil in initial concentrations start to deplete.

It is difficult to rationalize the initial behavior of the sensor due to the complicated composition of antioxidants and detergents. Initially the high temperature causes the sensor output to increase. At about 25 min at 180^0C a local maximum is observed and than the output signal starts to decrease. After about 60 min the sensors output becomes equal to the voltage seen with the new oil. This behavior could be hypothetically explained, first by the depletion of antioxidants, causing the signal to increase, and then, by the depletion of detergents, causing the signal to decrease. At this time, when detergents can not hold the oxidation products in suspension anymore, we can observe asymptotic behavior staring at the 60 minutes point.

After 60 min the hydrocarbon molecules continue to oxidize – for the interval from 60 to 1440 min. This behavior suggests that the concentration of the oxidized molecules in the adsorption layer increases and at some level will saturate. That will cause the sensor signal to stabilize at some new potential. From the experimental data it is possible to predict the saturation level at approximately 250 mV.

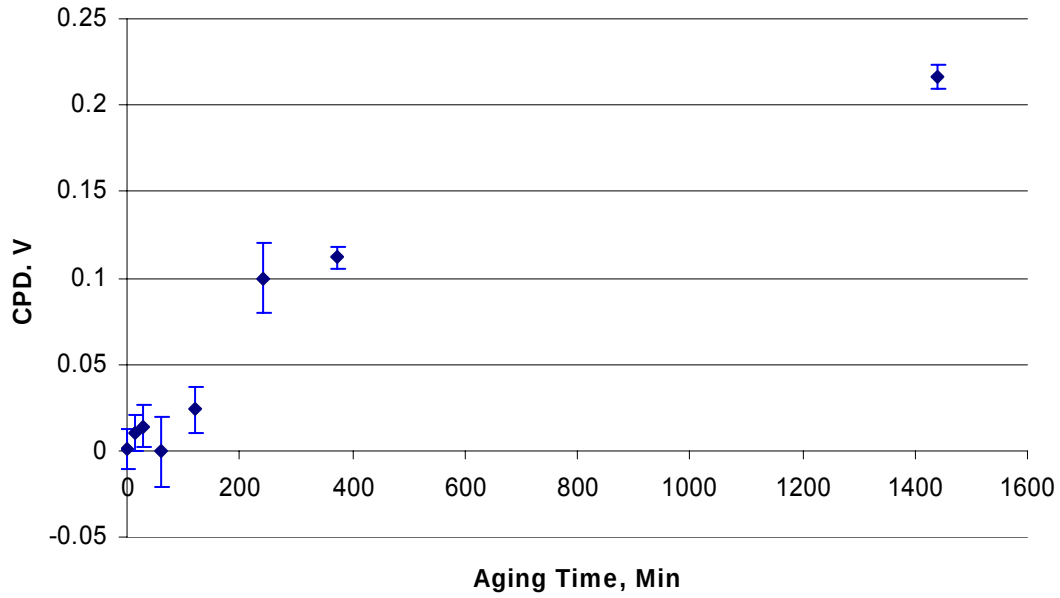

Figure 5-1: CDOS sensor output versus aging time

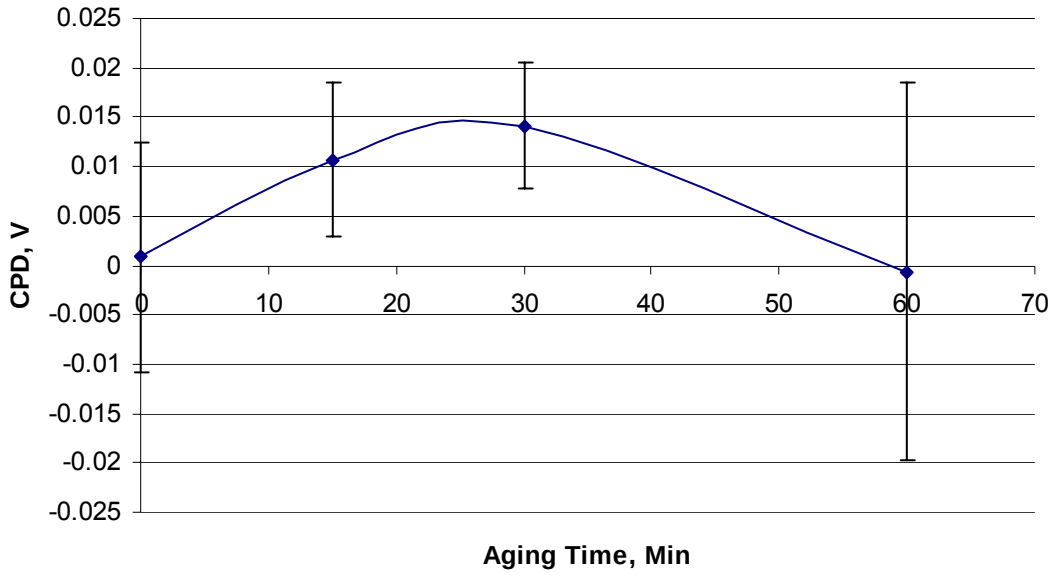

Figure 5-2: The CDOS sensor response corresponding to the first 60 min of aging

5.2 Oxidation of Base Stock

Motor oil, besides its direct lubricating purpose, serves as a coolant, corrosion protector, and method for removing contaminants from the engine filter. Loss of any essential function of the motor oil will lead to serious engine damage, if not either treated or noticed promptly. Through the oxidation process of motor oil, the key properties are destroyed. This type of degradation usually initiates severe damage to engine. The following changes in properties of motor oil are due to the oxidation of base stock: changes in physical properties (e.g. viscosity), changes in chemical properties (e.g. increased acidity). Average content of the base stock in the motor oil is on the level of eighty percent, therefore the degradation of the base stock is extremely dangerous for the engine [28].

The oxidation of the base stock is due to the free radical attacks against the main polymer chains, i.e. carbon hydrogen bonds. Figure 5-3 shows the chemical changes in the composition of the base stock.

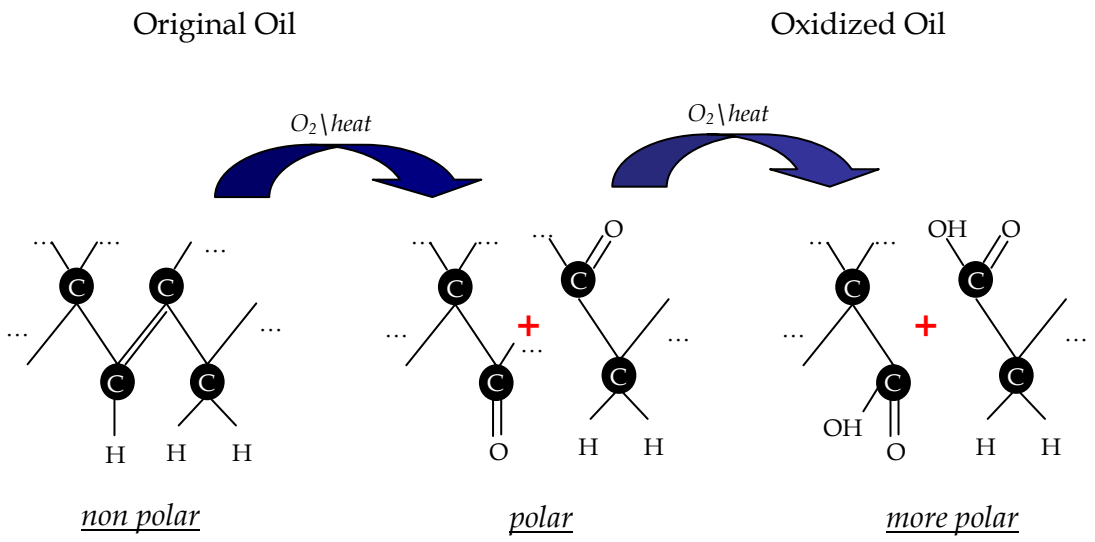

Figure 5-3: Oxidation of the base stock

In order to interpret the experimental data from the adsorption point of view an important assumption was made – the concentration of the oxidized molecules in the motor oil is proportional to the intentional oxidation time (i.e. aging time).

The experimental data plotted with the relative concentrations as the abscissa is shown on the Figure 5-4.

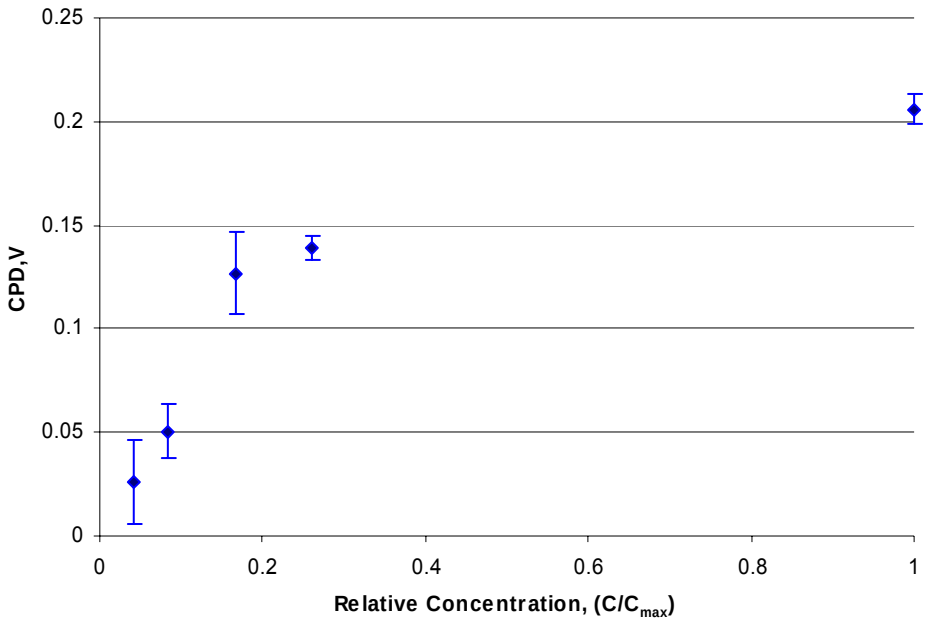

Figure 5-4: CDOS sensor output versus oxidized oil concentration

The asymptotic behavior of the output of the sensor is observed on Figure 5-4. This behavior is explained by the saturation of the surface of the metal where oxidized molecules adsorb. With increasing concentration of oxidized base oil less and less adsorption sites on the surface are available for other molecules to occupy.

From the experimental data, shown on the Figure 5-4, it can be concluded that the CDOS sensor is very sensitive to small changes in oxidized base stock concentrations and becomes less sensitive when concentrations reach higher levels.

5.3 Theoretical Model Fit to the Experiment

By use of the assumption made in Chapter 5.2, that the rate of oxidation of the motor oil is linear with time, the adsorption of the oxidized molecules onto the surface of the metal could be described by an adsorption isotherm. The Langmuir adsorption isotherm could be used as a basis to build a theoretical model for the results.

A minor modification of the Langmuir isotherm equation (2.9) was made to accommodate the experimental data. This modification is to incorporate the relative concentrations of the soluble molecules in the solution into the adsorption equation.

The real concentration C of the oxidized molecules is proportional to the relative concentration C' with the coefficient of proportionality τ :

$$C = \tau C' \tag{5.1}$$

Taking this into account, and introducing a new constant $K' = K\tau$, the Langmuir equation can be rewritten in the form (5.2).

$$\theta = \frac{K'C'}{1 + K'C'} \tag{5.2}$$

In order to relate the fractional coverage of the surface of the metal to the work function change of this metal due to the adsorption, the Helmholtz equation (2.22) was used. This equation states that there is a linear relationship between the normal component of the dipole moment of adsorbed molecule and a work function change. On the other hand, as shown by equation (2.23), the fractional surface coverage and the work function change also have linear relationship. Thus, the Helmholtz equation could be modified to the form (5.3).

$$\Delta(\Delta V) = \frac{\mu_N}{\varepsilon_r \varepsilon_0 A_M}\theta \tag{5.3}$$

where μ_N – is the normal component of the molecular/end-group dipole moment;

ε_r – the permittivity of motor oil;

ε_0 – the permittivity of free space;

A_M – the area of one molecule/end-group;

θ – the fractional coverage of the surface with oxidized molecules.

Finally the theoretical model for the adsorption of the oxidized oil on the surface of the metal could be written in the form (5.4).

$$V = V\big|_{C'=0} + \frac{\mu_N}{\varepsilon_r \varepsilon_0 A_M}\frac{K'C'}{1+K'C'} \tag{5.4}$$

where $V\big|_{C'=0}$ is a sensor's output voltage with a new sample, meaning that the concentration of the oxidized oil is equal to 0.

For simplicity, a new constant ξ (5.5) is introduced, and the equation (5.4) now can be rewritten as an equation (5.6).

$$\xi = \frac{\mu_N}{\varepsilon_r \varepsilon_0 A_M} \tag{5.5}$$

$$V = V\big|_{C'=0} + \xi\frac{K'C'}{1+K'C'} \tag{5.6}$$

The constants involved in this equation are of a very big importance. In this model they include both molecular and bulk properties of adsorbate, i.e. normal component of dipole moment, area of molecule, and dielectric constant, adsorption energy and etc.

The fit of the theoretical model to the experimental data was done and the following values for the constants were obtained to be $\xi = 0.229[\mathrm{V}]$ and $K' = 3.833$. The corresponding calculations and methodology for obtaining constants could be found in the Appendix II.

Figure 5-5 shows a comparison of the experimental data and the results of the theoretical model.

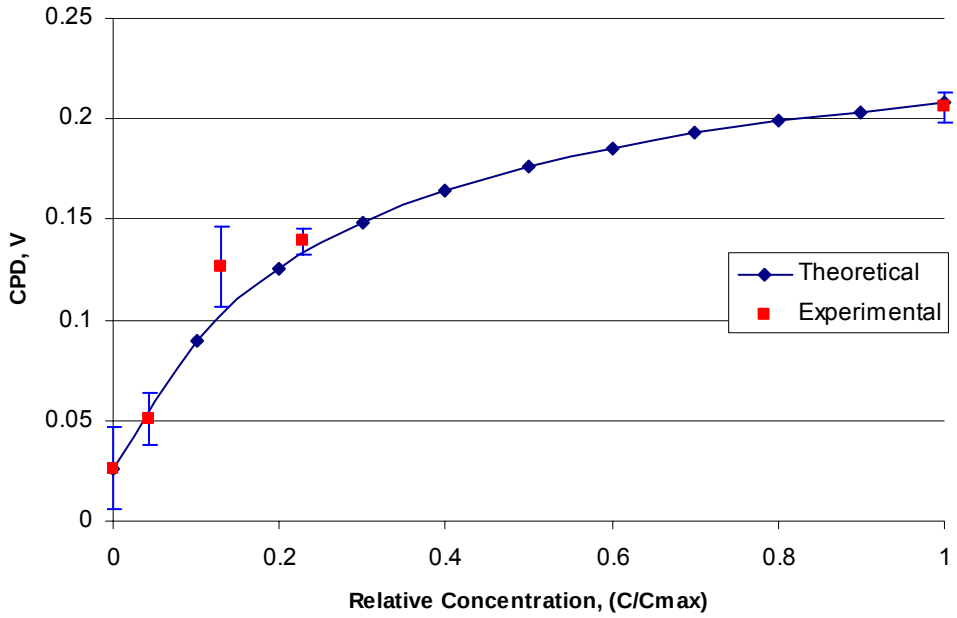

Figure 5-5: Theoretical prediction versus experimental data

A good correlation between the experimental data and theoretical model can be observed. This behavior could be expected because the experimental data was used to calibrate the coefficients for the model.

Using the obtained constants the important relationship relating the normal component of dipole moment and area of molecule could be obtained using equation (5.5). Substituting values for ε_r and ε_0 relation was obtained (5.7).

$$\frac{\mu_N}{A_M} = 4.0476 \times 10^{-12} [C/m] \qquad (5.7)$$

Relationship (5.7) allows the determination of the normal dipole component of the adsorbed molecule if one knows the area of the adsorbate. On the other hand if one knew the area of the adsorbate, it is easy to calculate the normal component of dipole moment.

Due to the limited access to the information about the base oil used in MOBIL-1 motor oil, it was not possible to calculate either the dipole moment or the area of the base stock. But an attempt to approximate those parameters was made and is shown in the next section.

5.4 Molecular Dipole Moment Effect

The molecular dipole moment plays very important role in molecule behavior. Its adsorption, electrical and dielectric properties are substantially influenced by the dipole moment. It was shown in chapter 2.4.3 than the work function change of the metal due to the adsorption of a substance on the surface is proportional to the normal component of the molecule dipole moment of the substance.

The molecular orientation on the surface during adsorption is defined by the magnitude of the dipole moment and the amount of charge stored in the surface. Therefore charged surfaces tend to align molecules at the surface. Moreover the surface with extensive charge will create an electrical double layer and align sometimes up to several molecular layers. Depending on the magnitude of the dipole moment of the molecules, the surface charge will be spread away from the surface, more or less.

The long chain molecules, e.g. the motor oil base stock molecules, possessing different radicals due to degradation, can preferentially adsorb on the surface with a particular end-group. The dipole moment of the end-group adsorbed on the surface will dictate the amount of change in the surface potential – bigger dipole moment of that group then the more developed the change will be.

It was discussed in the chapter 5.2 that the main products of the oxidation of the base oil are the carboxyl groups. This end-group is more polar than the carbonyl group, so the fair assumption will be that the adsorption on the surface happens mostly with carboxyl groups.

V.J. Novotny and T.E. Karis in their experiments with perfluoropolyether (PFPE) films were able to calculate the dipole moment for the carboxyl group of the Z-diac PFPE to be 0.9D. [33]

Korach, Streator and Danyluk (2001) [17] calculated the area of the molecule of PFPE to be 0.785E-18 m^2. Not claiming to be a good approximation of the area of molecule of the base stock for MOBIL 1, this molecule area was used to calculate the dipole moment of the carboxyl group based on the experimental data and the developed theory.

The relationship between the normal component of dipole moment and the area of molecule adsorbed on the surface of the sensor is represented by equation (5.7). Substituting the assumed area of molecule in the model we obtain the value for the dipole moment of carboxyl group to be equal 0.95D.

The proximity of the obtained value to the value calculated in [33] should not be considered a proof of the preferential adsorption of carboxyl groups on the surface. Too many assumptions were made to conclude this. But it is enough to justify the plausibility of the theoretical model. In order to finalize the conclusion about which

molecular group is preferential in adsorption, its orientation, it is necessary to run additional experiments. Polarization reflection IR spectroscopy is a common method for analyzing molecular configuration on metal surfaces, for instance parallel or perpendicular orientation of molecules, with regard to adsorbent surfaces.

CHAPTER 6

CONCLUSIONS

This research showed a novel application of the Vibrating Kelvin Probe in the form of the developed Vibrating CPD Chemical Degradation Oil Sensor, that can be used for either monitor or asses the level of oxidation in the lubricant.

The major conclusions of this thesis are as follows:

1. The CDOS sensor was proved to be extremely sensitive to the level of oxidation in the lubricant. It is capable of detecting the difference between new oil and oil which has been intentionally oxidized for 15 minutes at 180^0C.
2. The CDOS sensor was capable of seeing changes in concentrations of antioxidants and detergents in motor oil.
3. The output of the CDOS sensor follows an asymptotic behavior with the increasing aging time, corresponding to the oxidation of the base stock.
4. An important relationship between the normal component of dipole moment and the area of adsorption was obtained in the following form:

$$\frac{\mu_N}{A_M} = 4.0476 \times 10^{-12} [C/m]$$

5. Based on several assumptions, it was determined that the oxidized base stock adsorbs on the surface of the metal preferentially with carboxyl groups. The calculated dipole moment for this end-group equal to 0.95D, which is very close to the published in literature 0.9D.

CHAPTER 7

RECOMMENDATIONS

To further improve this system, the following recommendations were compiled and shown below.

- An online sensor may be developed based on CDOS sensor described in this thesis. Special precautions should be taken into account when designing the online sensor. It was noticed that the online application, for instance a flow system, influences the vibration parameters of the piezo-vibrator and unbalances the lock-in amplifier. Moreover, the two plates should be manufactured from two dissimilar metals and one of them electrically isolated to prevent shortening.
- A more refined model describing multilayer adsorption needs to be developed. The Brunauer, Emmett, Teller (BET) model could be used to predict the coverage and the number of layers participating in adsorption.
- A more detailed experimental analysis of the adsorption needs to be performed by use of appropriate techniques, e.g. polarization reflection IR spectroscopy, in order to determine true orientation of molecules.
- Samples with different additives may be analyzed using the CDOS sensor. Oxidation, rust inhibitors, dispersants, detergents, anti-wear additives, and viscosity improvers are the potential additives which may be monitored by the CDOS sensor.

APPENDIX I

LABVIEW PROGRAM CODE

The block diagram of the virtual instrument is shown in Figure A1-1.

As it could be seen from the diagram, the virtual instrument has a cascade structure or film structure with frames. The frames are executed consequently. During the first time frame the secondary window of GUI is updated showing the any auxiliary signal. Next time frame the main acquisition is being run; obtained data is being formatted and written to a file.

Two sub-VIs are presented on the diagram. They are *"Logger Sub VI"* and *"Auxiliary Check Sub VI"*. On the diagram they are represented by the sub-VIs with icons according to Figure A1-2. These modules directly work with the hardware: configure and control it.

The block diagrams for these sub-VIs are shown in Figure A1-3 and Figure A1-4.

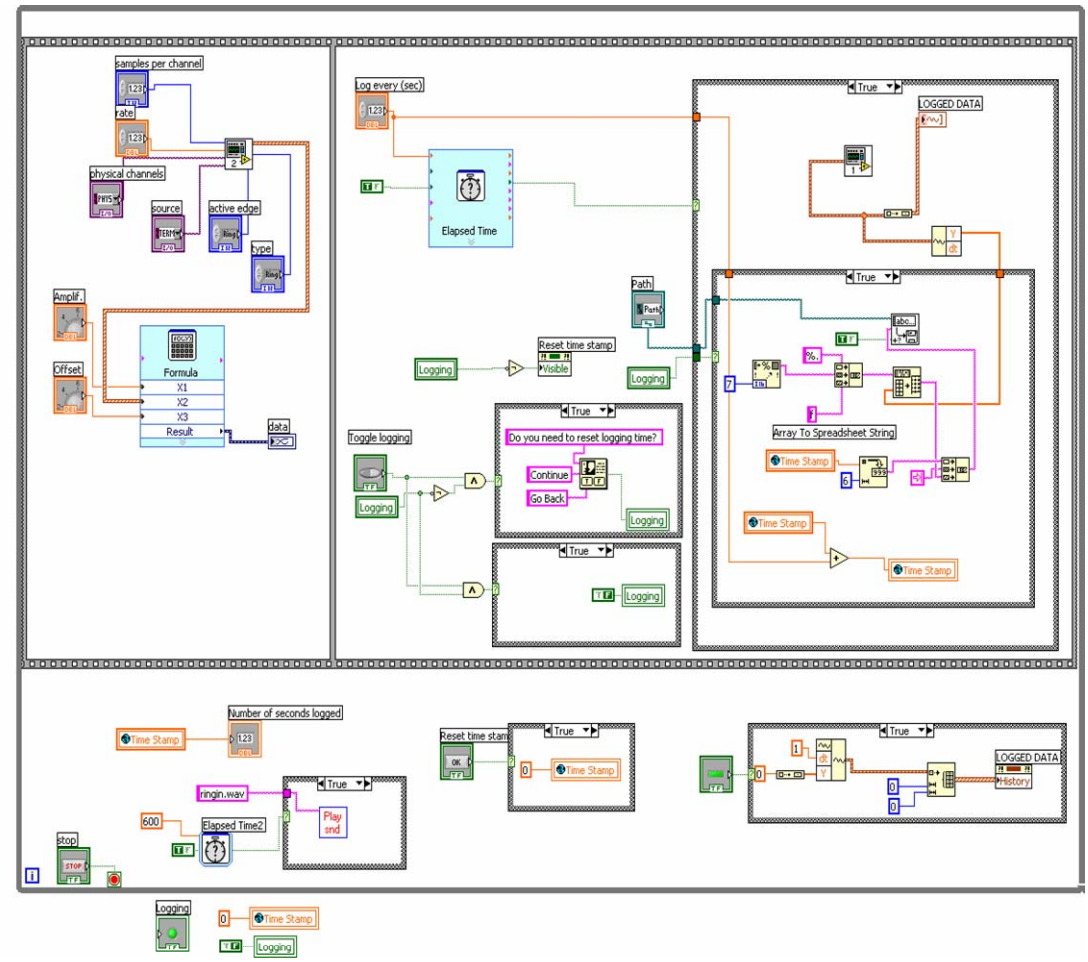

Figure A1-1: Block diagram of the developed virtual instrument

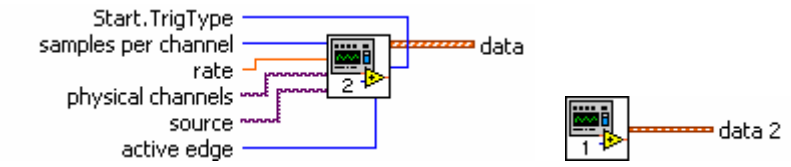

a) Auxiliary sub VI *b) Logger sub VI*

Figure A1-2: Developed Sub VI Icons in Labview

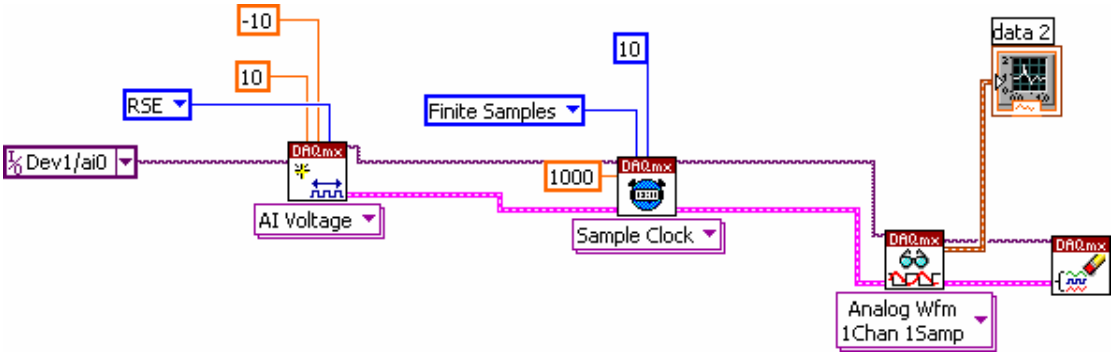

Figure A1-3: Logger sub VI

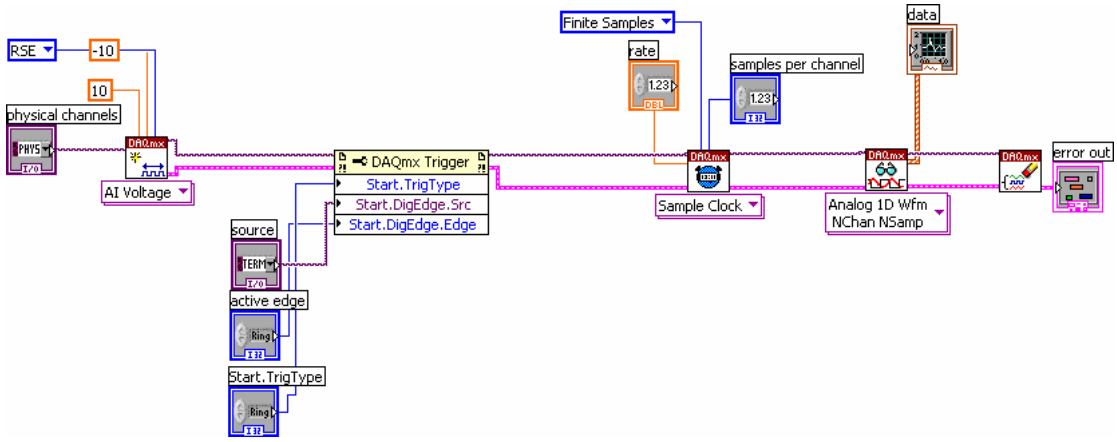

Figure A1-4: Auxiliary check sub VI

APPENDIX II

THEORETICAL MODEL FOR THE CDOS SENSOR

As it is shown in the chapter 5.3 the theoretical model for the CDOS sensor could be presented in the following way:

$$V = V\big|_{C'=0} + \xi \frac{K'C'}{1+K'C'} \tag{A2.1}$$

where

$$\xi = \frac{\mu_N}{\varepsilon_r \varepsilon_0 A_M} \tag{A2.2}$$

In order to calculate ξ and K' from the data fit of the equation (A2.2) to the experimental data, the following rearrangement was done:

$$\frac{C'}{V - V\big|_{C'=0}} = \frac{1}{K'\xi} + \frac{1}{\xi} C' \tag{A2.3}$$

Data plotted in the form of (A2.3) should look linear with a slope equal $\frac{1}{\xi}$ and intersect the y-axis at the point $\frac{1}{\xi K'}$.

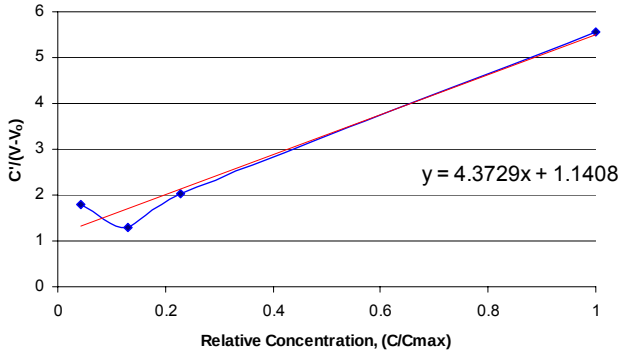

Figure A2-1: Reciprocal plot for experimental data

Figure A2-1 shows the obtained plot and the least square linear fit [32] to it. The plot corresponds to the following value of $V\big|_{C'=0} = 0.128\text{V}$. The following values for $\frac{1}{\xi}$ and $\frac{1}{\xi K'}$ were obtained:

$$\begin{aligned} \frac{1}{\xi} &= 4.3729[V^{-1}] \\ \xi &= 0.229[V] \\ \frac{1}{\xi K'} &= 1.1408[V^{-1}] \\ K' &= 3.833 \end{aligned} \tag{A2.4}$$

Using the empirical constants obtained, (A2.4), it is possible to calculate the ratio between the normal component of dipole moment and area of adsorbed molecule for the experiment, equation (A2.5).

$$\frac{\mu_N}{A_M} = 4.0476 \times 10^{-12}[C/m] \tag{A2.5}$$

APPENDIX III

T-NETWORK EQUIVALENT RESISTANCE

High ohmic value resistors superimpose substantial thermal noise onto the signals. T-network feedback is a well known technique to increase the effective feedback resistance while having small value resistors. Another application of this method can be found when the required value resistors are not available and small values are used together with T-network to achieve the same result. Figure A3-1 shows the circuit diagram for T-network feedback [34].

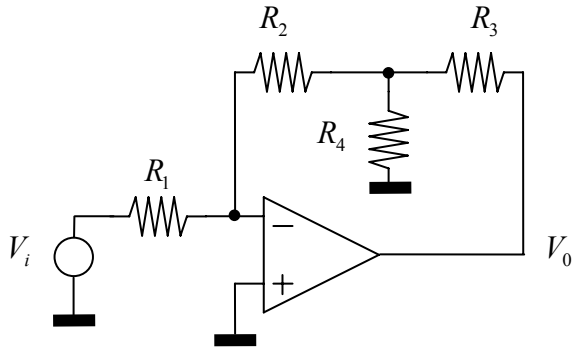

Figure A3-1: T-network feedback

$$A = \frac{V_0}{V_i} = -\frac{R_2}{R_1}\left(1 + \frac{R_3}{R_4} + \frac{R_3}{R_2}\right) \qquad \text{(A3.1)}$$

The gain of the inverting amplifier can be calculated using formula (A3.1). Furthermore, using the properties of the inverting amplifier circuit, the equivalent feedback was obtained to be equal to R_{eqiv} (A3.2).

$$R_{eqiv} = R_2\left(1+\frac{R_3}{R_4}+\frac{R_3}{R_2}\right) \qquad \text{(A3.2)}$$

R_1 and C_1 on Figure 3-1, chapter 3.3.1, form a low pass filter with the cutoff frequency 250Hz. The capacitor at the frequency above 250Hz can be neglected and the input stage will look like the one shown in Figure A3-1. After substituting values from the circuit diagram into (A3.2) the equivalent resistance is:

$$R_{eqiv} = 10^9\left(1+\frac{470\cdot 10^3}{12\cdot 10^3}+\frac{470\cdot 10^3}{10^9}\right)Ohm = 4.01\cdot 10^{10}\,Ohm \qquad \text{(A3.3)}$$

BIBLIOGRAPHY

1. Lord Kelvin, Phil. Mag. 46, 82 (1898)
2. Volta A., Ann. Chim. Phys., 40, 225 (1801)
3. Zisman W.A., Rev. of Sci. Instr., 3, 367 (1932)
4. Freidel J. The physics of clean metals surfaces. Ann. phys., 1, 6, p. 257-307 (1976)
5. Scott W.T. The physics of Electricity and Magnetism, (1966)
6. Zharin A.L. "Method of Contact Potential Difference and its Applications in Tribology", 1996
7. Philosophical Transactions, vol. 90, pt. I, p. 405
8. Zanoria E., Hammall K., Danyluk S., Zharin A., KSTLE, 11,40,(1995)
9. Hiemenz P.C., Principles of colloid and surface chemistry.
10. Rosen, Milton J., Surfactants and interfacial phenomena. – 3rd ed. (2004)
11. Beltzer M. ASME J. Tribol., 114, 675 (1992)
12. Pekar S.I, Tomasevich O.F. "Thermoelectronic emission from metals covered with thin layer of semiconductor", *Journal of Technical Physics* 17,12 (1947) p.1339-1342
13. Atkins P.W. Physical Chemistry 5th ed, p.849 (1994)
14. Gottlieb M.H. J. Phys. Chem –US. 64, 4, p. 427-432
15. Gaines G.L. Jr. Insoluble Monolayers at Liquid-Gas interfaces, Interscience, 1966
16. Phillips G., J. Sci. Inst., 28, 342 (1951)

17. Korach C.S., Streator J., Danyluk S., Applied Physics Letters, 75, 5, p.698-700 (2001)

18. Yano D., Korach C., Streator J., Danyluk S., ASME J. Tribol. 121, 980 (1999)

19. Troyer D., Fitch J., Oil analysis basics. (2001)

20. Goodlive S.A., Lvovich V.F., Humphrey B.K., Boyle F.P., On-board Sensor Systems to Diagnose Condition of Diesel Engine Lubricants – Focus on Soot. (2004)

21. Carey A.A., Hayzen A.J., The dielectric Constant and Oil analysis", Practicing Oil Analysis Magazine (2001)

22. Baumgartner H., Liess H.D., Rev. Sci. Instrum, 59(5), (1988)

23. Rossi F., Rev. Sci. Instrum, 63(7), (1992)

24. Baikie I.D., Estrup P.J., Rev. Sci. Instrum, 69(11), (1998)

25. Baikie I.D., Mackenzie S., Estrup P.J.Z., Meyer J.A., Rev. Sci. Instrum, 62(5), (1991)

26. Baumgartner H., Hornung U., Lieb H.D., Ederle E., Archiv fur Elektrotechnik 76, 265-271 (1993)

27. Saito S., Soumura T., Maeda T., J. Vac. Sci. Technol. A 2(3), (1984)

28. Korus, R.A.; Mousetis, T.L.; Lloyd, L. Polymerization of Vegetable Oils. *American Society of Agricultural Engineering,* (1982**),** Fargo, ND, 218-223

29. Hadjadj A., Roca P, Equer B., Rev. Sci. Instrum. 66(11), (1995)

30. Lundgren S., Kasemo B., Rev. Sci. Instrum. 66(7), (1995)

31. Baikie I.D., Venderbosch E., Meyer J.A., Estrup P.J.Z., Rev. Sci. Istrum. 62(3), (1991)

32. Faires J.D., Burden R. Numerical Methods, 2nd ed. (1998)

33. Novotny V.J., Karis T.E., Appl. Phys. Lett., 71, 1, (1997)

34. Franco S., Design with operational amplifiers and analog integrated circuits, – 3rd international ed. (2002)